2018

# A Route to Fabricate Rapid and Efficient Dye-sensitized Solar Cells through Minimizing the Duration of TiO2 Film Disposition and Dye Sensitization

Md Ataul Mamun
*South Dakota State University*

# A ROUTE TO FABRICATE RAPID AND EFFICIENT DYE-SENSITIZED SOLAR CELLS THROUGH MINIMIZING THE DURATION OF $TiO_2$ FILM DEPOSITION AND DYE SENSITIZATION

BY

MD ATAUL MAMUN

A thesis submitted in partial fulfillment of the requirements for the

Master of Science

Major in Electrical Engineering

South Dakota State University

2018

A ROUTE TO FABRICATE RAPID AND EFFICIENT DYE-SENSITIZED SOLAR CELLS THROUGH MINIMIZING THE DURATION OF $TiO_2$ FILM DEPOSITION AND DYE SENSITIZATION

MD ATAUL MAMUN

This thesis is approved as creditable and independent investigation by a candidate for the Master of Science degree and is acceptable for meeting the thesis requirement for this degree. Acceptance of this thesis does not imply that the conclusions reached by the candidate are necessarily the conclusions of the major department.

Qiquan Qiao, Ph.D. Date
Major Advisor

Brian Logue, Ph.D. Date
Thesis Advisor

George Hamer, Ph.D. Date
Acting Head, Department of Electrical Engineering and Computer Science

Dean, Graduate School Date

# ACKNOWLEDGEMENTS

I would like to express my sincere gratitude to Dr. Qiquan Qiao for supervising me in this thesis. I am equally grateful to Dr. Brian Logue for his enormous support and guidance throughout the course of my research work, and for his time and effort for improving the quality of this thesis. I am thankful to Dr. Parashu Kharel and Dr. Huitian Lu for being in my committee and reviewing my thesis.

I am very much indebted to Mr. Jason Sternhagen and Mr. Dan Flaskey for their helps to upgrade the functionalized carboxylate deposition (FCD) instrument.

I would also like to thank all my research group members, faculty members, staffs and students of LARGE Lab at Chemistry and Biochemistry Department and Center of Advanced Photovoltaics at the ECE department of South Dakota State University for their direct and indirect helps.

Finally, I would like to thank my wife (Hosni Ara Tanjim), son (Tammam Abrar), other family members and my friends for their endless support and being always with me regardless of my good and bad times.

TABLE OF CONTENTS

# ABBREVIATIONS

AFM: Atomic Force Microscopy

CE: Counter electrode

DSSC: Dye Sensitized Solar Cell

EQE: External Quantum Efficincy

FCD: Functionalized Carboxylate Deposition

FF: Fill Factor

FTO: Fluorine-doped tin oxide

FWHM: Full Width Half Maximum

HOMO: Highest Occupied Molecular Orbital

IPCE: Incident photon-to-current conversion efficiency

ITO: Indium tin oxide

LAN: Local Area Network

LUMO: Lowest Unoccupied Molecular Orbital

MFC: Mass Flow Controller

MW: Microwave

NREL: National Renewable Energy Laboratory

PCE: Power Conversion Efficiency

UV-Vis: Ultraviolet-Visible

XRD: X-ray Diffraction

# LIST OF FIGURES

# ABSTRACT

## A ROUTE TO FABRICATE RAPID AND EFFICIENT DYE-SENSITIZED SOLAR CELLS THROUGH MINIMIZING THE DURATION OF $TiO_2$ FILM DEPOSITION AND DYE SENSITIZATION

MD ATAUL MAMUN

2018

Dye Sensitized Solar Cell (DSSC) technology is considered a promising substitute to the conventional silicon-based solar cells due to DSSC's low material cost, ease of fabrication, low toxicity, and relatively high power conversion efficiencies. The two major steps of DSSC fabrication are: 1) formation of a mesoporous $TiO_2$ layer on a transparent conductive oxide (TCO) coated glass substrate to make its photoanode, and 2) sensitization of the photo-anode with dye. Conventionally, photoanodes are prepared by depositing a mesoporous $TiO_2$ layer on a TCO-coated glass substrate and sintering at a high temperature (~450 °C) for 30-60 minutes. The prepared $TiO_2$ is then dip-coated in a dye solution for ~24 hrs. These processes have remained unchanged for almost 27 years and require more than 90% fabrication time of a typical DSSC. Thus, they limit the throughput and cost-effectiveness of this technology. This thesis introduces a novel technique to rapidly form mesoporous $TiO_2$ films on FTO (fluorine doped tin oxide)-coated glass substrates using microwave irradiation with essentially identical performance as conventional heating. Microwave (MW) assisted films were prepared at

low temperatures (< 260 °C) within less than 10 minutes. DSSCs fabricated with 8 minutes of MW irradiated films show similar efficiencies with that of conventionally fabricated DSSCs. Besides saving time, and energy compared to its counterpart, this approach may pave the way of plastic-based electronics. This thesis also demonstrates the rapid (< 30 minutes) loading of two Functionalized Carboxylate Deposition (FCD) dyes through high vacuum (0.1 mTorr) FCD. The power conversion efficiency (PCE) achieved with the FCD DSSCs were higher than dip-coated DSSCs. Combinedly, microwave-assisted photoanode preparation, and FCD dye-sensitization can save more than 90% fabrication time for future ultra-low cost DSSCs.

# Chapter 1. Introduction

## 1.1 Background

Energy, which played a massive role in the evolution of human civilization, has now become an integral part in day-to-day life. People use energy in many activities such as cooking, transportation, lighting, food production and storage etc. For centuries fossil fuels like coal, natural gas, and petroleum have been acting as the primary source to meet world's energy demand. Burning of these fossil fuels affects the environment by producing greenhouse gas that causes climate change, pollutes air that impacts human health [1]. Moreover, these energy sources are limited, and non-renewable as natural formation of fossil fuels takes millions of years. But, the energy consumption is increasing day by day with the increase in population and the development of human life style. The worldwide energy demand is expected to be doubled by 2050, and tripled by the end of this century [2]. In this context, it is necessary to invent ways to utilize renewable and clean energy sources such as solar, wind, tidal currents, biomass, geothermal energy etc. to reduce the uses of fossil fuels. Besides, helping in meeting the increasing energy demand, the renewable and clean energy sources can ensure environmental sustainability unlike conventional energy sources.

The sun is a massive renewable energy source which is inexhaustible, ecofriendly, and omnipresent. Each year, the earth receives around $3x10^{24}$ J of solar energy which is approximately ten thousand times more than the global energy consumption by the entire population per year [3]. However, the sun delivers the energy in the form of

electromagnetic radiation which requires a conversion in a suitable form (e.g. electrical energy) for versatile uses of human.

Solar cells can convert sunlight into electricity. At present, most of the commercial solar cells are produced from crystalline silicon. The price of electricity generated by the state-of-the-art silicon-based cells is significantly more than that of the electrical grid [4]. This is mainly due to the higher manufacturing costs of the silicon-based cells. Thus, alternate and cheap sources of solar cells are in search.

Due to low material and production cost, simple fabrication technique and relatively high performance, the dye sensitized solar cells (DSSCs) have attracted tremendous attention as an alternative to silicon-based solar cells [5-7]. A typical DSSC has four main parts: a photo anode of mesoporous/nanocrystalline $TiO_2$ layer, a sensitizing dye, an electrolyte, and a counter electrode [8]. Two major steps of fabricating DSSCs are: formation of a mesoporous $TiO_2$ layer on a transparent conductive oxide (TCO) coated glass substrate to make the photoanode, and sensitization of the photo-anode with dye. Despite much evolution in production technique of DSSCs, the conventional methods of preparing the photoanodes by high temperature (~450 °C) sintering of mesoporous $TiO_2$ layer on TCOs for 30-60 minutes [9-11], and ~24 h dip-coating of the photoelectrodes in a dye solution [12], have remained unchanged for almost 27 years. These two steps taking more than 90% of the fabrication time, remain as a limiting factor of the technology. Therefore, there is a need for an alternative and efficient way to replace these techniques.

## 1.2 Previous Work

In the early 1990's O'Regan and M. Gratzel reported the first modern DSSCs with an improved efficiency of 7.9%. The photoanodes of the DSSCs were based on nanocrystalline $TiO_2$ [13]. Since this pioneering work, the nc-$TiO_2$ has been used as a standard nanostructured semiconducting scaffold for the photoanodes of DSSCs [14]. However, the conventional preparation of mesoporous/nc-$TiO_2$ films by sintering at 450-500 °C for 30-60 min remain unchanged since the very beginning. Inspired by the successful engagement of microwave processing in synthetic chemistry, Vigil *et al.* first demonstrated the growth of $TiO_2$ compact layer in solution on ITO substrates in 1999 [16]. However, their method required significantly more materials than required in the film (as the substrate was dipped into the solution), and they did not show any applications. In 2004 Hart *et al.* reported that direct exposure of the TCOs in microwave irradiation shattered the TCO-coated glass substrates [17]. So, they applied low microwave power to prepare a $TiO_2$ blocking layer on the FTO/glass and applied it to DSSCs. However, the maximum power conversion efficiency (PCE) they achieved was only 2.8% with the microwaved films [9]. In 2012, Jayan *et al.* showed that the film developed in solution using microwave irradiation was not uniform [18] and they found good agreement between the grown film patterns and their electromagnetic simulations. These experiments suggest that a novel technique is required to protect the TCO/glass substrates in direct microwave irradiation to rapidly grow uniform mesoporous $TiO_2$ film on the TCOs for their application in DSSCs.

O'Regan and M. Gratzel el al., in their seminal work on DSSC in 1991, dip coated the photoanodes in Ruthenium-based dye solution for sensitization to achieve an

efficiency of 7.1-7.9% [19]. Since then, sophisticated ruthenium based DSSCs showing PCEs more than 11% [20] looked very promising. However, due to their high cost, complex synthesis and purification processes, and low molar extinction coefficients, researchers pay attention to synthesize metal-free organic dyes as an alternative [8, 21]. Researches synthesized a series of organic dyes with good overall efficiency, however, like metal-based dyes the sensitizing method (dip-coating for 16-24h) of these organic dyes remained unchanged [8] and continued to be a limiting factor. Besides consuming huge time, the dip-coating has other disadvantages, such as it necessitates the use of organic solvents, leads to dye waste, and often causes inefficient sensitization. Mathew *et al.* reported 13% PCE for molecularly engineered porphyrin dye. They dipped the photoanodes in dye solution for a relatively short period of time (6 hours) [22]. However, this process used toxic and volatile organic solvents and still consumed a major portion of the fabrication time. Baral *et al.* at SDSU introduced functionalized carboxylate deposition (FCD), a gas phase deposition technique of particular organic dyes, as an alternative way of forming dye monolayer on $TiO_2$ in 2014 [23]. They used relatively low vacuum (~180 Torr) which could not be used for high molecular weight organic dyes. Santosh *et al.* improved the vacuum to ~500 mTorr of the FCD system and fabricated DSSCs using two relatively low-molecular weight (MW < 340 g/mol) dyes and achieved efficiencies similar to the dip-coating [24]. However, those dyes were themselves inefficient. Hence, there is a need to fabricate FCD-based DSSCs with efficient FCD dyes through improving the vacuum system.

## 1.3 Motivation

Rapid deposition of $TiO_2$ mesoporous layer as well as quick sensitization of photoanodes is expected to endow a fast and ultra-low cost DSSC production technique.

## 1.4 Objectives

1. To develop microwave-assisted nano-crystalline $TiO_2$ films on FTO substrates within 10 minutes
2. To compare microwave-deposited nc-$TiO_2$ films with that of conventionally deposited nc-$TiO_2$ films using standard characterization techniques and apply the films in DSSCs to evaluate their functionality.
3. To improve the vacuum of the FCD system to achieve at least 0.1 mTorr pressure within 15 minutes
4. Sensitize photo-anodes using FCD with organic dyes of molecular weight more than 420 g/mole for DSSCs to achieve an overall efficiency similar to or more than dip-coated counterpart
5. Sensitize microwave assisted $TiO_2$ photoanodes in FCD method; fabricate DSSCs and evaluate their performances

# Chapter 2. Microwave-assisted rapid and low-temperature preparation of mesoporous-$TiO_2$ film

## 2.1 Introduction

### 2.1.1 Background

Metal oxide films have gained research interests in thin film technology. Among them titanium dioxide ($TiO_2$) films have attracted tremendous attention with numerous applications including photo-catalysis [25], solar cells [26], self-cleaning windows [27], gas sensors [28], Li-ion battery photo-anodes [29], photodetectors [30], and protective coatings [15]. Multiple studies have reported that preparation of nc-$TiO_2$ film on the transparent conductive oxide (TCO) coated substrates requires high temperature annealing (450-500 °C) for 30-60 minutes [16-18]. This is required to achieve good interparticle connection between $TiO_2$ particles within the film and between the $TiO_2$ and the TCO-coated substrate such as the FTO. Without this excellent connection, the $TiO_2$ produces poor charge-transport properties. The high temperature long sintering time and associated cool down time of around 40 minutes limit the manufacturing throughput and consumes a relatively large amount of energy. A rapid and low temperature method to grow films can save time and energy and may ultimately lead to the ability to grow nc-$TiO_2$ on plastic-based substrates.

In contrast to conventional heating, microwave heating is fast, selective, and has the ability to quicken reactions [31]. Because of these features, it has a broad application in synthesis of organic and inorganic materials [32]. Researchers have tried to engage it in thin film processing on FTO/ITO coated glass substrates. However, the FTO/ITO-

coated glass substrates shatter almost instantly when exposed to microwave irradiation at a conventional operating frequency of 2.45 GHz. Substrates shatter as the TCO-coatings absorb microwave radiation much more efficiently compared to glass which was described by Uchida et. al in 2004 [33] and Hart et. al in 2005 [17]. As an alternative way, Reeja Jayan *et al.* demonstrated microwave-assisted low temperature $TiO_2$ thin film growth on indium tin oxide (ITO) substrates from solution in 2012 [18] which was pioneered by Vigil et. al in 2000 [16]. However, the method produced highly non-uniform films at a deposition duration of ~1 hour. The non-uniformity of these films was based on growth in solution, where film growth was spontaneous. Also, film deposition method from dipping in solution with microwave required more materials than needed in the film. An alternative and efficient way would be screen print the $TiO_2$ layer on TCO and directly irradiate microwave. Thus, a special effective technique is necessary to protect the TCO substrate.

This work demonstrates the production of nc-$TiO_2$ films on FTO-glass substrates via microwave irradiation within 8 minutes. The films were characterized via standard techniques and compared to conventionally sintered nc-$TiO_2$ films. This study demonstrates the functionality of the nc-$TiO_2$ anodes by fabricating and characterizing the performance of DSSCs produced with microwave developed films.

### 2.1.2 Motivation

Direct microwave irradiation is expected to grow nc-$TiO_2$ films on FTO-coated glass rapidly in a low-temperature to save time, and energy to develop DSSC photoanodes.

### 2.1.3 Objectives

1. To develop a technique to protect FTO-glass from shattering in direct microwave irradiation
2. To develop microwave-assisted nano-crystalline $TiO_2$ films on FTO-glass substrates within 10 minutes
3. To compare microwave-deposited nc-$TiO_2$ films with that of conventionally deposited nc-$TiO_2$ films using standard characterization techniques and apply the films in DSSCs to evaluate their functionality.

## 2.2 Theory

### 2.2.1 Introduction to microwave

Like visible light or radio waves, microwaves are a form of electromagnetic energy with wavelengths ranging from 1 mm to 1 m (frequencies of 300 GHz to 300 MHz respectively), lying between infrared and radio waves. Figure 2.1 shows the microwave range in the electromagnetic spectrum. Generally, microwaves are widely used for wireless communications such as cellular network, wireless local area network (LAN), standard (Wi-Fi), RADAR and space craft communication, GPS communications etc. [34]. Besides, communication uses, microwaves are also extensively used for heating at industry and at home. However, a large portion of the microwave band is retained for communication purpose, and generally two frequencies are used for heating: 915 MHz and 2.45 GHz [35].

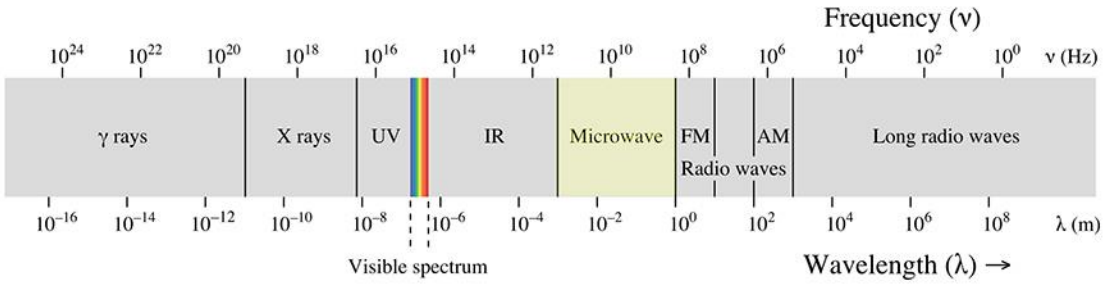


Figure 2.1. Microwave range in the electromagnetic spectrum [36]

Heating using microwave irradiation delivers several advantages over conventional heating, such as microwaves directly convey their energy to the target material without convention or conduction (which are the main processes of conventional heating). Thus, microwave heating is faster and selective [34].

2.2.2 Microwave heating

MW irradiation can transfer heat mainly by two mechanisms: ionic conduction, and dipolar polarization [37]. In ionic conduction free electrons and ions move freely in response to an applied microwave and collide each other to heat up [18]. In dipolar polarization microwaves rotate the molecules of a material having permanent or induced dipoles. Molecules of materials with high dielectric loss collide each other for dipole rotation during polarization and are heated up. This heat loss is defined as absorbed power and can be calculated from Equation 2.1 [38, 39]

$$P = (2\pi f)\varepsilon_0 \ddot{\varepsilon} E^2 V \quad (2.1)$$

Where, f is the frequency of the wave, $\varepsilon_0$ is electrical permittivity in space, $8.854 \times 10^{-12}\ F/m$, $\ddot{\varepsilon}$ is the dielectric loss factor (depends on the heating material), E is the applied electric field, V is the volume of the material.

So, heating with microwave depends on the material's dielectric loss factor. Depending on the dielectric loss factor, materials can be generally classified into three groups [32].

Microwave absorptive: These materials absorb microwave excellently and generate heat within it. Examples: Water, wood, rubber etc.

Microwave reflective: These materials reflect microwave and are not heated up. Generally, they are used for waveguides. Bulk metals (Al, Fe etc.), alloys fall in this category.

Microwave transparent: These materials are transparent to microwave, and heat is not generated within them when microwave passes through them. Quartz, PTFE belong to this group.

### 2.2.3 Penetration depth/skin depth

When an electromagnetic radiation is incident on the surface of a material, it may partly reflect from that surface and partly transmit into the material. In a real metal/conductor, the electric and magnetic fields and current decay exponentially with distance from the surface of the conductor, a phenomenon known as the skin effect. The distance is called skin depth or penetration depth. For a given material, penetration depth will generally be a function of wavelength.

### 2.2.4 Film characterization

#### 2.2.4.1 UV-Visible Absorption

When visible light (with adjacent ranges) falls on a material, some portion of the light is absorbed. The absorption depends on the length/thickness, concentration, and type of the material. A material absorbs UV-Visible light means it undergoes electronic transitions i.e. the light excites the electrons from ground state to the excited state [40]. Absorption is also a function of the wavelength of incident light. The amount of absorbance, at different wavelengths, can be measured with a UV-Visible spectrometer.

#### 2.2.4.2 Raman scattering and spectroscopy

When a monochromatic light falls on a molecule whose net dipole moment is zero, it scatters a light that is of slightly different frequency (higher or lower) due to its change in polarizability [41] (Figure 2.2). This scattering is called Raman scattering. This

scattered light frequency, which is unique to the molecule, is the signature of that molecule. By detecting and matching that frequency, the molecule can be identified. Raman spectroscopy is a technique that is based on this inelastic scattering of light. This technique is used to observe vibrational, rotational, and other low-frequency modes [42]. It is complementary to IR spectroscopy and commonly used in chemistry to identify molecules.

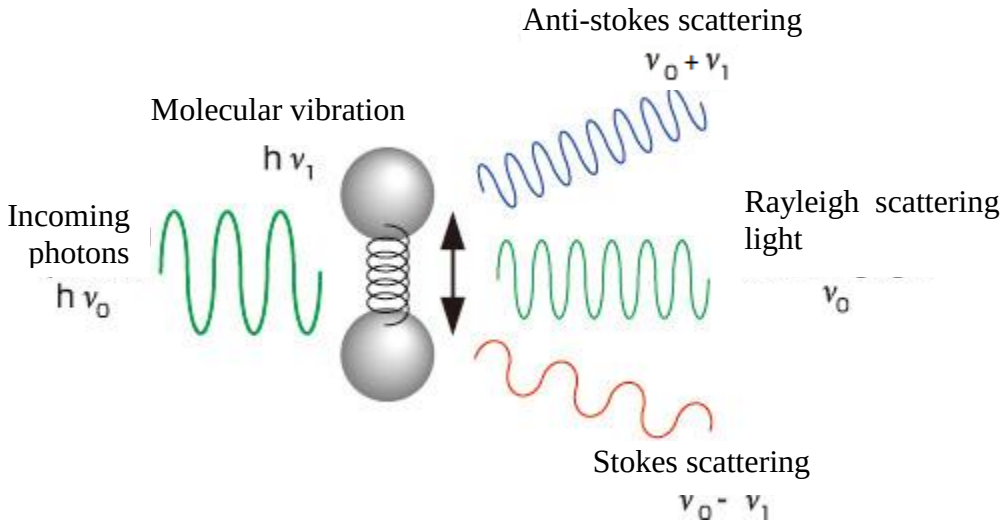


Figure 2.2. Raman scattering [43]

2.2.4.3 X-ray diffraction

When an X-ray beam falls on a crystal, the atoms diffract the beam into many specific directions. By measuring the intensities and angles of the diffracted X-ray beams the crystal structure can be known. X-ray crystallography is used to determine the atomic and molecular structure of a crystal [44]. It also provides information on phase, preferred crystal orientation (texture), and other structural parameters, such as average grain size, crystallinity, strain, and crystal defects. It is one of the most prominent non-destructive technique to analyze materials in form of powders, fluids, or crystals. X-ray diffraction can be understood by Bragg's Equation.

$$n\lambda = 2d\ sin\theta \qquad (2.2)$$

Where, n is an integer, d= interplanar spacing, $\theta$ is the X-ray angle of incidence, $\lambda$

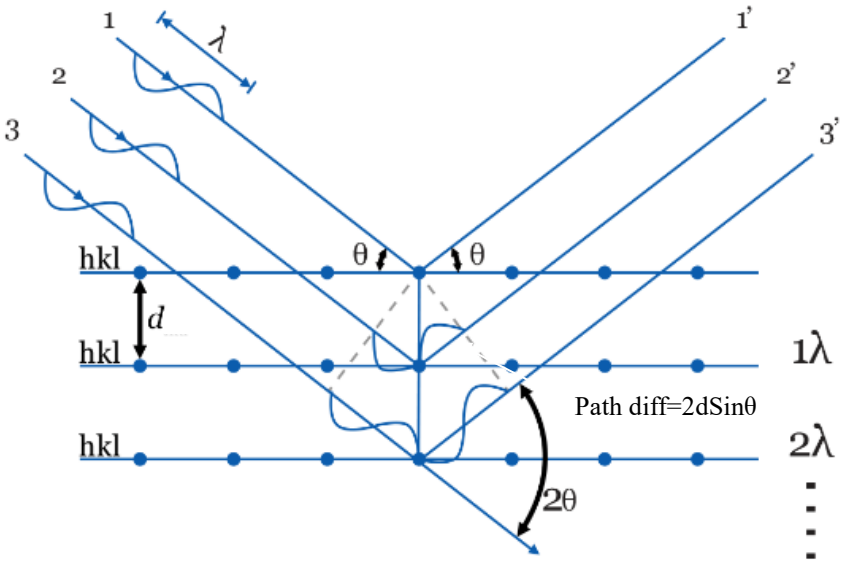


Figure 2.3. Calculating interplanar distance with Bragg's law [45]

is the X-ray wavelength. Knowing the constructive interference angle, $\theta$ for ray 1 and ray 2 of Figure 2.3, the interplanar distance can be measured from Equation 2.2.

2.2.4.4 Atomic Force Microscopy

Atomic force microscope (AFM) is a kind of scanning probe microscope to measure surface topography [46]. Generally, it possesses a very high resolution, on the order of fractions of a nanometer. It operates by measuring force between its tip and the sample and can measure surface topography, material composition and characteristics, height, friction, magnetism.

A typical AFM consists of a cantilever with a sharp tip at its free end, a diode laser, a photo-detector, and a piezoelectric scanner as shown in Figure 2.4.The tip scans a sample surface. When the tip is brought into proximity of a sample surface, forces between the tip and the sample lead to a deflection of the cantilever according to Hooke's law. The deflection is measured with laser beam which is reflected to photo-detector from the top surface of the cantilever. With the help of photodiode and computer, corresponding information can be decoded.

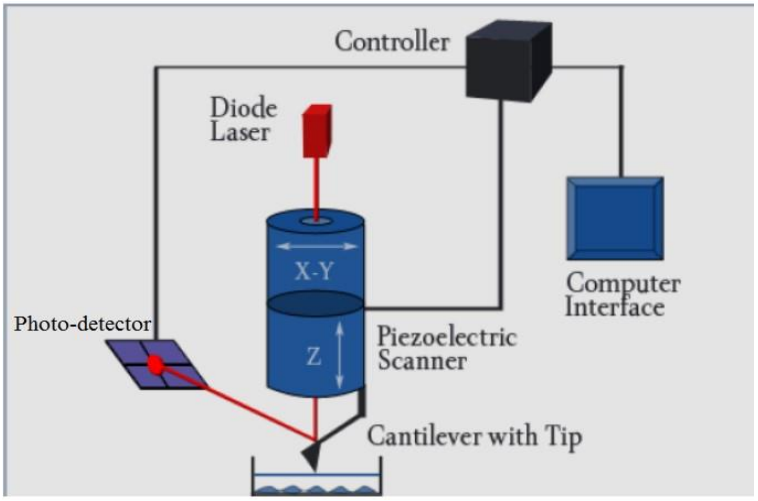


Figure 2.4. Schematic diagram of a typical AFM [23]

AFM has three modes of operation depending on the tip-sample distance: 1) contact mode, 2) non-contact mode, and 3) tapping mode. The net force between the tip and sample can be attractive or repulsive. In contact mode, AFM tip touches the sample surface and repulsive force between the tip and sample deflects the cantilever. In non-contact mode, the tip does not touch the sample surface and works in the attractive regime. In tapping mode, AFM tip touches the sample surface intermittently and operates in both attractive and repulsive force regime. The modes of operations with the force regimes are shown in Figure 2.5

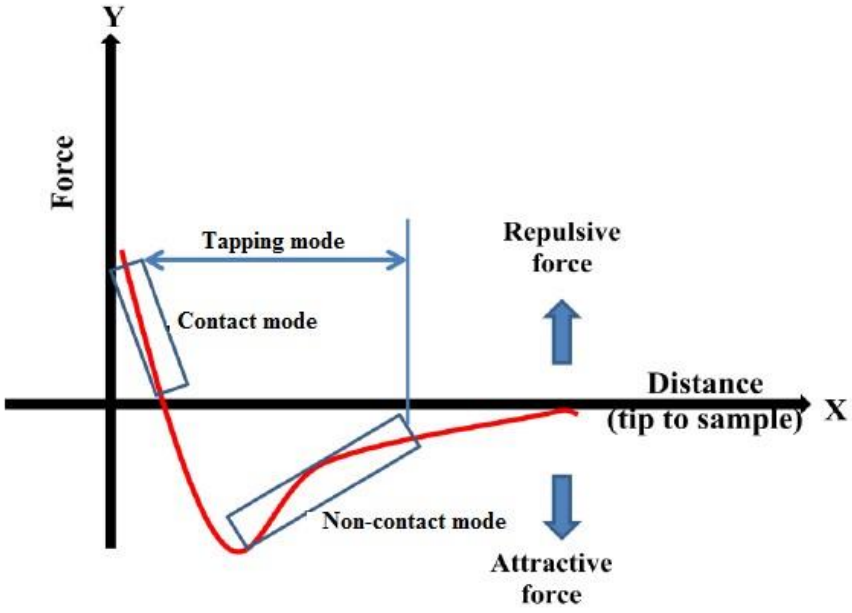


Figure 2.5. AFM operating modes [23]

In tapping mode cantilever is oscillated externally to its resonance frequency. The tip-sample interaction changes the oscillation magnitude as well as the resonance frequency. The deviations of the amplitude and frequency from the reference amplitude and frequency are used as a feedback signal to the controller for surface imaging [47].

## 2.3 Experimental Procedures

The following tasks were performed to achieve objectives of this work

1. Engage thin Al foil to border the FTO-coated glass substrate to protect FTO-glass from cracking in microwave irradiation and deposit nano-crystalline $TiO_2$ film using microwave irradiation.
2. Investigate the MW develop film with UV-Vis absorption spectroscopy, Raman spectroscopy, XRD crystallography, and Atomic Force Microscopy.
3. Observe the performance of the MW developed films by applying them to fabricate DSSCs.

### 2.3.1 Materials

FTO-glass substrates (50 mm x 50 mm x 3 mm) were purchased from Solaronix, Aubonne, Switzerland. The substrates were then cut into 25 mm x 25 mm x 3 mm shape to use as standard substrates in microwave reactor. Nanocrystalline $TiO_2$ (Ti-Nanoxide T/SP), Electrolyte $I_3^-/I^-$ were also acquired from Solaronix, Switzerland. A microwave reactor of General Electric Co., (model#JES1358WJ, 1.65 KW, 2.45 GHz) was used for experiments.

### 2.3.2 Development of mesoporous film with microwave irradiation

Prior to deposition, the FTO-coated glass substrates were cleaned by sonication in a detergent solution, deionized (DI) water, acetone, and 2-propanol each for around 15 min, followed by a 15 min UV cleaning. Screen printing was used to deposit a mesoporous $TiO_2$ layer of around 1.5 cm x 1.5 cm on the FTO-coated glass substrates to develop nc-$TiO_2$ films of thickness of ~6 µm. These films were used for UV-Vis

spectroscopy, Raman spectroscopy, XRD, and AFM. To prepare photo anodes for DSSCs, a layer of 0.25 $cm^2$ was screen printed on FTO coated glass substrates to produce an nc-$TiO_2$ film. Before placing inside the microwave chamber, the samples were bordered with thin Al foil, to protect the FTO-glass substrates from cracking, as shown in Figure 2.6. The sample was then placed in a nonconductive ceramic vial and the vial was placed inside the microwave chamber. 4, 6, and 8 min MW films were prepared using 4, 6, and 8 consecutive microwave irradiation periods. Each irradiation period constitutes of 50 s active microwave irradiation (100% power) and 10 s relaxation (0% power).


Figure 2.6. FTO-glass substrate bordered with Al foil to use inside MW reactor

An IR temperature sensor (Fluke-561) was used to measure temperature of the sample by holding it at about 5 cm from the substrate. Before dipping into the dye solution, the photo-anodes were cooled down inside the reactor chamber, unassisted, for around 10 minutes.

### 2.3.3 Development of mesoporous film with conventional method

The cleaning and screen printing method used for microwave irradiation were applied to deposit a mesoporous $TiO_2$ layer on the FTO-coated substrates after cleaning. The substrates were then sintered at 450 °C for ~30 min. Before dipping into the dye solution, the photo-anodes were cooled, unassisted for around 30 minutes.

### 2.3.4 DSSC fabrication

The prepared photoelectrodes were soaked in a 0.3 mM N-719 dye solution in anhydrous ethanol for 24 h to attach dye molecules with $TiO_2$ particles. After dye loading, the photoanodes were rinsed with acetonitrile to remove unattached dye molecules from the $TiO_2$ surface. The counter electrode (CE) was prepared by spin coating a platinum solution at 2000 rpm for 10 s on FTO-coated glass followed by sintering at 450 °C for 15 min. The CEs were assembled with the photoanodes using a thermoplastic sealant. The $I_3^-/I^-$ electrolyte solution was then injected in between the photoanode and counter electrode through reserved a channel.

### 2.3.5 Characterization and Evaluation

#### 2.3.5.1 UV−vis absorption spectroscopy

An Agilent 8453 UV−vis spectrophotometer with ‘Chemstation software’ (Figure 2.7) was used to acquire UV- Vis absorption spectra to compare the MW-developed $TiO_2$ films and conventionally annealed $TiO_2$ films on FTO-coated glass. UV-Vis spectra were captured using a bare FTO-glass as background. This spectrophotometer was also used to measure the absorption spectrum of the L1 and L2 dyes soaked from the photoanodes of the FCD cells and conventionally fabricated cells.

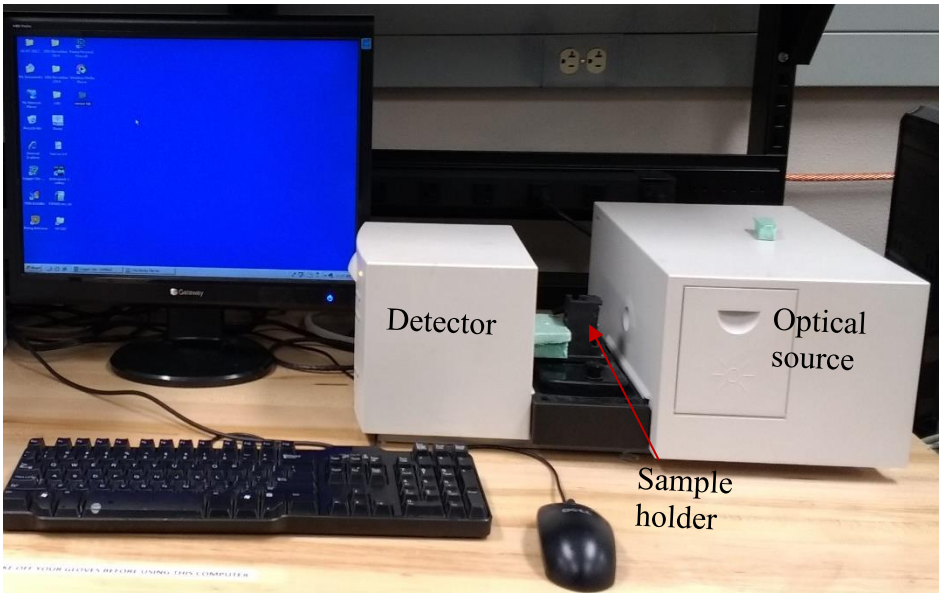


Figure 2.7. Agilent 8453 UV-Visible spectrophotometer

2.3.5.2 Raman spectroscopy

A Horiba Jobin Yvon Raman spectroscope (Figure 2.8) was used to perform Raman spectroscopy for MW-developed nanocrystalline $TiO_2$ films as well as conventionally annealed nanocrystalline $TiO_2$ films.

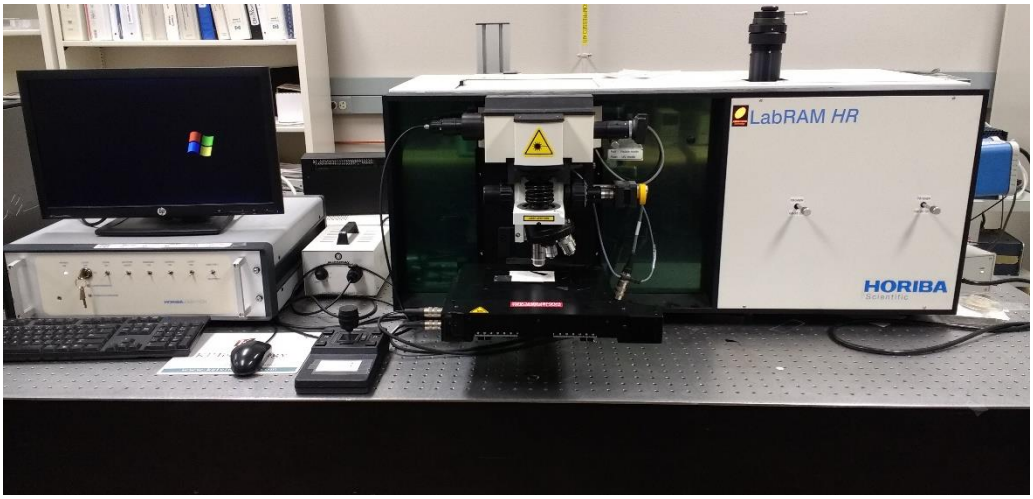


Figure 2.8. Horiba Jobin Yvon Raman spectroscope

2.3.5.3 XRD crystallography

XRD crystallography was performed using a Rigaku Smartlab X-ray (Figure 2.9) diffractometer for the MW developed mesoporous $TiO_2$ films as well as for conventionally-heated mesoporous $TiO_2$ films.


Figure 2.9. Rigaku Smartlab X-ray diffractometer

2.3.5.4 Atomic Force Microscopy

Topographic images of the MW developed nc-$TiO_2$ films as well as conventionally annealed nc-$TiO_2$ films were captured using an Agilent 5500 AFM (Figure 2.10) containing Budget Sensors TAP 300 Al tip. Tapping mode was used with 75 kHz resonant frequency. The tip was in net attractive force. Imaging was performed at room temperature and humidity for all the samples. Gwyddion 2.45 image processing software was used to analyze the images.

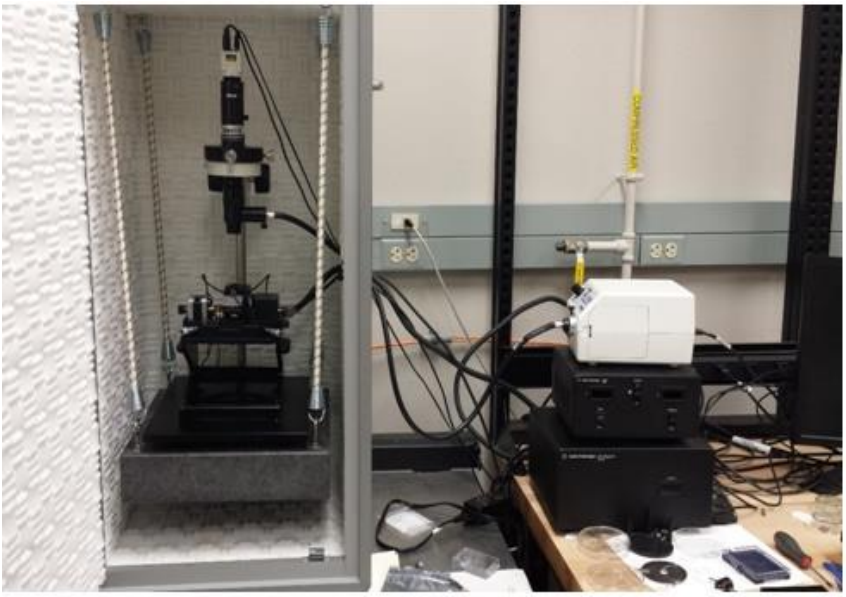

Figure 2.10. Agilent 5500 scanning probe microscope [23]

## 2.4 Results and Discussion

Different materials with different dielectric loss factor absorb different power. Glass is almost microwave transparent [17, 32] and $TiO_2$ absorbs microwaves moderately [48]. However, the conductive coatings such as FTO and ITO absorb microwave extremely well [18] which ultimately results in shattering the substrate [17, 48]. The rapid change in temperature of the FTO compared to glass, causes rapid breakage of the substrate (Figure 2.11b). Generally, cracks begin from the edges of the substrates. It was hypothesized that attenuation of microwave radiation as well as heat transfer from the FTO to the glass near the edges would reduce the temperature difference at the edges and stop the glass from breaking. As metal has the dual capability of blocking MW [32, 49] and transferring heat, we select thin (~10 μm) aluminum foil to border substrate. The ratio of the attenuated intensity to the original intensity for a pure Al sheet of thickness 10 μm can be calculated from Beer-Lambert law as shown in Equation 2.3, which we found around 0.28%.

$$I = I_0\, e^{-z/\delta} \tag{2.3}$$

Where, $I_0$ is the microwave intensity at the surface, I is the microwave intensity after penetrating the Al foil, z is the measured thickness of Al foil =~10 μm, $\delta$ is the penetration depth of pure Al at 2.45 GHz = 1.7 μm [34]

Besides attenuation of microwave irradiation, the Al foil would minimize the temperature difference by conducting thermal energy from substrate top to bottom. Figure 11c and d show the use of the Al foil and the resulting FTO-coated glass substrate before and after microwave irradiation. The resulting intact substrate (i.e., no cracks observed) would be

useful as photoanode, whereas the substrate in Figure 11b (i.e., unprotected FTO-coated glass) would be unusable because of the multiple cracks apparent.

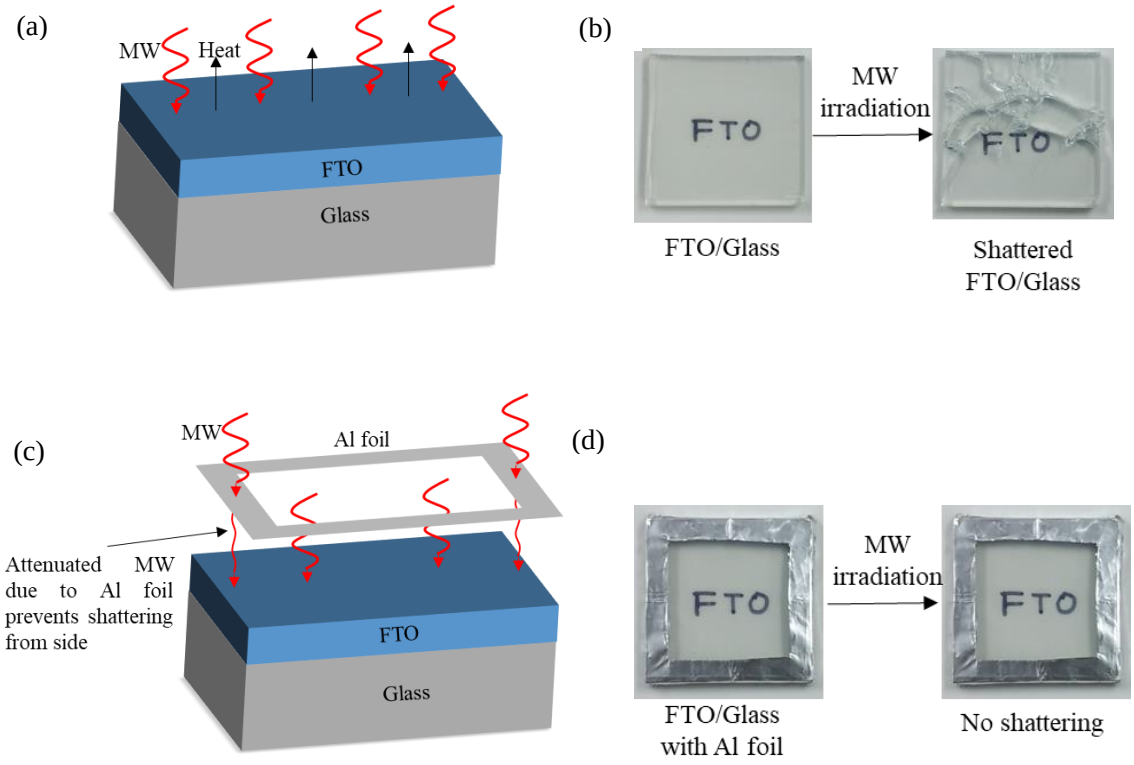


Figure 2.11. MW interaction with the FTO-glass with and without Al foil (a) FTO coating absorbs microwave to heat up quickly (b) FTO coated glass shatters quickly when exposed in microwave (c) Thin Al foil attenuates microwave that supposed to hit the boarders of the substrate to protect the substrate from cracking (d) FTO-coated substrate bordered with thin Al foil remains intact in microwave exposure.

To ensure further endurance (in long duration of MW irradiation) by minimizing temperature difference between substrate's top and bottom, it was placed into a ceramic vial which also absorbs a portion of microwave energy. The other purpose of the ceramic vial was to protect the MW reactor's magnetron by acting as a dummy load by absorbing MW energy inside the chamber.

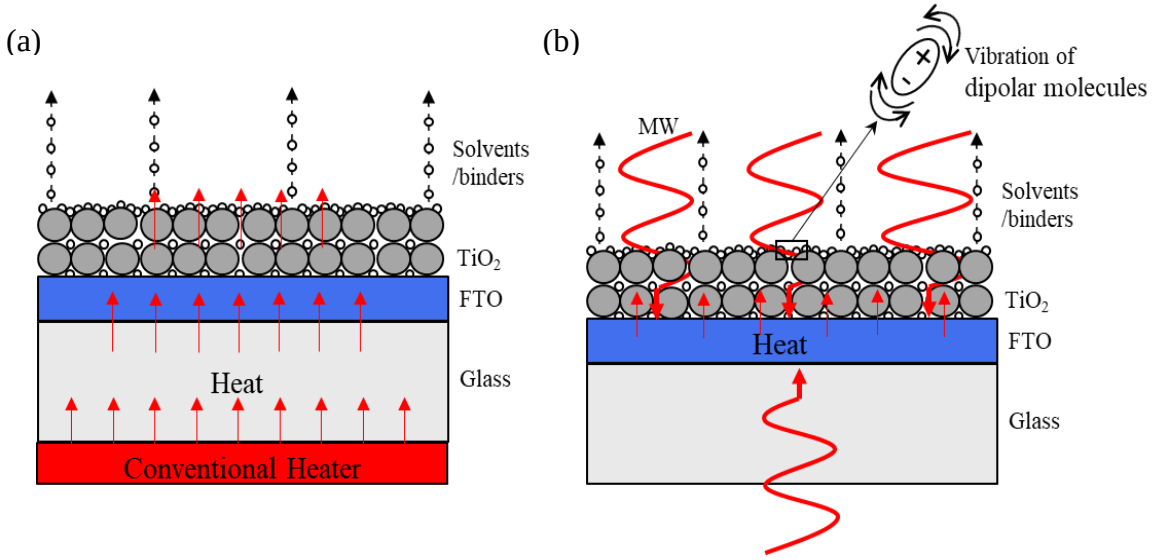


Figure 2.12. $TiO_2$ sintering (on FTO) using conventional heating and MW irradation (a) Conventional heating is inefficient as the heater heats itself to transfer heat and a significant portion of heat does not reach the target. (b) MW-assisted heating is efficient as FTO and solvent/ binders can separately heat up to evaporate solvents, and prepare the $TiO_2$ crystal

Since the FTO coating is a major microwave absorbing medium on glass substrates, only a small amount of energy is needed to prepare a nc-$TiO_2$ film. Very small thickness of FTO coating (only around 400-500 nm [50, 51]) means it absorbs a small amount of MW energy while its direct contact with $TiO_2$ means effective and efficient heat transfer unlike conventional heater. Conventional heating (Figure 2.12 (a)) is based on conduction and convection principle where the energy transfer is slow, and inefficient [37]. For MW irradiation, even though the FTO is heated up quickly it is low enough

(260 °C) compared to 450-500 °C conventional annealing temperature for the concerned period of reaction. Figure 2.12 (b) shows the FTO layer predominantly absorbs microwave irradiation to sinter the $TiO_2$ and to evaporate solvents and binders.

The vibration of $TiO_2$ molecules as well as the heat transferred from the FTO coating accelerates the reaction to form a rapid crystal and to bind $TiO_2$ layer on the FTO. Furthermore, the organic binders and solvents also absorb microwave irradiation [52, 53] which accelerates their evaporation. Thus, microwave interaction leads to localized energy absorption, heating, and subsequent nucleation and growth of a desired film [18]. Figure 2.13 shows the comparison between the high temperature conventional annealing and low temperature short time microwave irradiation to form nc-$TiO_2$ films.

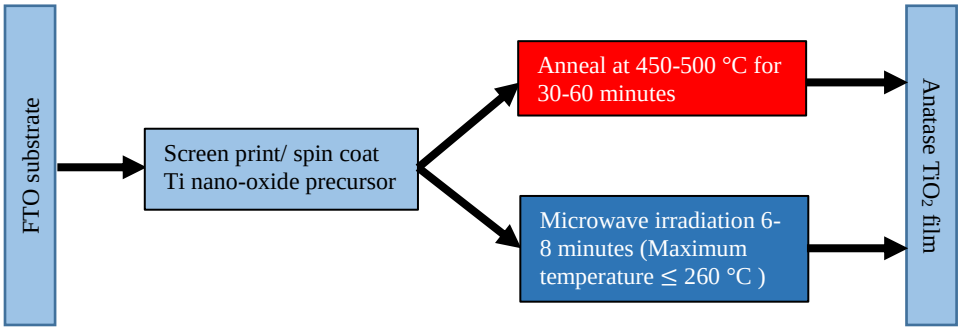


Figure 2.13. Comparison of nc-$TiO_2$ film forming routes on FTO-coated substrates via conventional annealing and microwave irradiation

The nc-$TiO_2$ paste contains organic binders and other solvents such as terpinol. Initially it appears slightly bluish-white. With heating it gradually turns black and then off-white with continued heating (Figure 2.14 a). The color change to black indicates combustion of the binders, with subsequent evaporation of the combustion products to produce an off-white nc-$TiO_2$ film indicates a binder/solvent free film. UV-Vis absorption spectroscopy was used to examine whether the films are free from unwanted solvents and binders (i.e., these organic components degrade the electron-transport capacity of the nc-$TiO_2$ films).

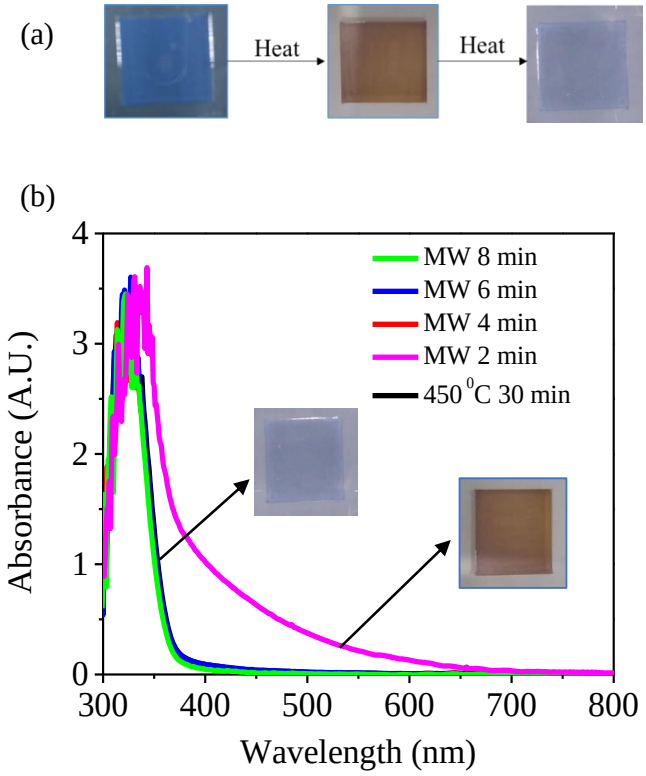


Figure 2.14. Heating effect on $TiO_2$ paste, and corresponding UV-Vis spectra (a) Color change of $TiO_2$ mesoporous paste with heating (b) UV-Vis absorbance spectra of

conventionally annealed and microwave irradiated films. Insets: $TiO_2$ paste color with heating.

Figure 2.14 b shows the UV-Vis absorption spectra of conventionally annealed (~450 °C 30 min) film is virtually identical to the MW irradiated films (for 4, 6, and 8 min) with an absorption peak at around 325 nm wavelength. For comparison absorption spectra of a 2 min MW-irradiated film is presented which is easily distinguishable from the 4, 6, and 8 min MW and the conventionally annealed films. Visually these films look similar unlike the black 2 min microwaved film.

For conventional annealing, the first visible darkness observed at a temperature around 200 °C, whereas for microwave irradiation it is observed at less than 100 °C. The changing of paste color at low temperature with microwave irradiation might be due to organic binders' high absorption of microwave energy. Microwave heating is selective [18], unlike conventional annealing, so it is possible that the organic precursors absorb microwave very well and subsequently degrade and evaporate. Also, as the FTO layer heats up quickly with microwave, it transfers the heat to the film.

Figure 2.15 shows the Raman spectra of conventionally annealed film and microwave irradiated films. The FWHMs (Full Width Half Maximum) of all films are almost same. Peaks centered around 144 $cm^{-1}$, 197 $cm^{-1}$, 399 $cm^{-1}$, 519 $cm^{-1}$, and 639 $cm^{-1}$ confirm the presence of anatase phase. No evidence of the rutile phase of $TiO_2$ was seen. Moreover, the transformation from anatase to rutile phase happens at a temperature higher than 500 °C [54] which is much higher than produced during the MW irradiation preparation of nc-$TiO_2$ film.

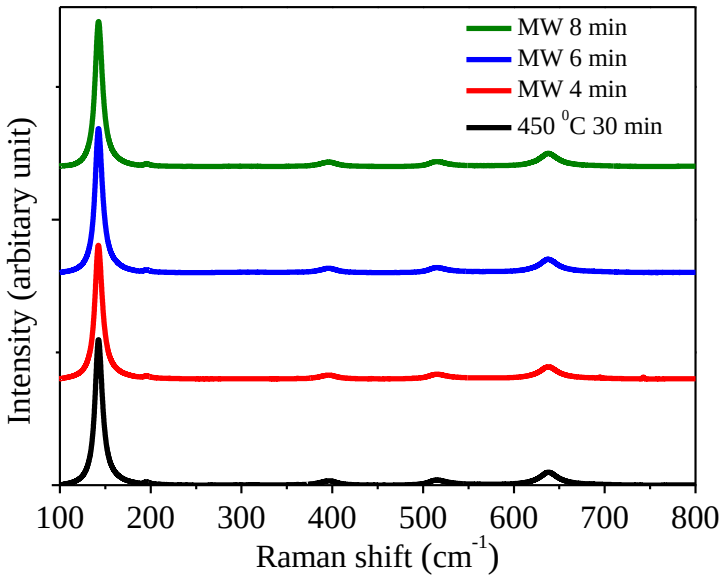


Figure 2.15. Raman spectra conventionally annealed film and microwave irradiated films

For further assurance about crystallinity of the microwave prepared films XRD was used. Figure 2.16 shows the X-ray diffraction patterns of $TiO_2$ films prepared with the conventional method and microwave irradiation on FTO-coated glass. All the patterns

are identical with only one phase (anatase) in existence with prevalence of planes corresponds to (101) at 25.28, (105) at 53.84, and (200) at around 48.38.

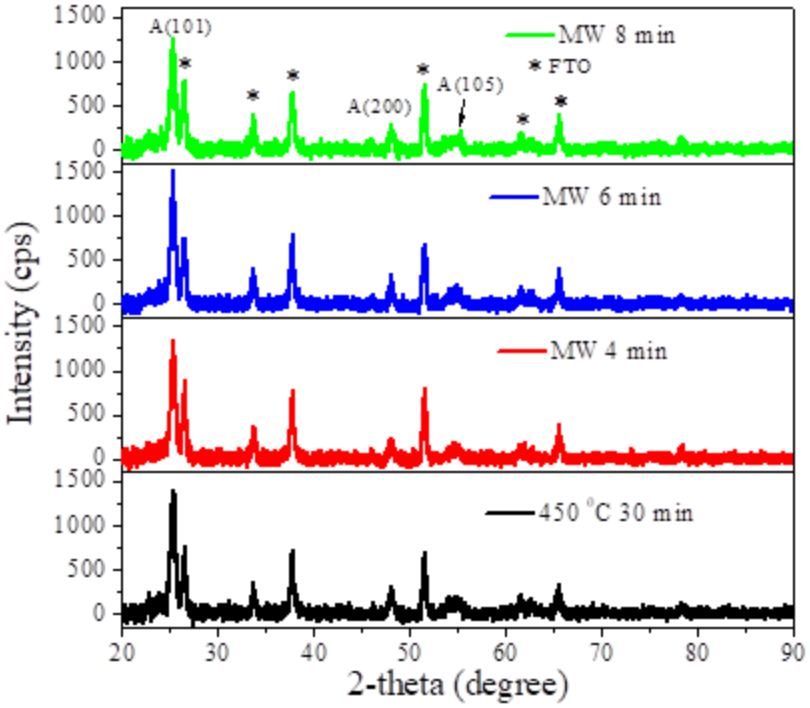


Figure 2.16. XRD spectra of microwave irradiated films and conventionally annealed films

Crystal sizes of the microwave developed films and the conventionally annealed films were estimated using Scherrer's Equation. The full width at half maximum (FWHM) and corresponding crystal size for the prevalent (101) peak are shown in Table 2.1.

Table 2.1. Particle sizes of nc-$TiO_2$ films acquired by conventional heating and microwave irradiation

| Heating method | FWHM | Particle size (nm) |
|---|---|---|
| 450 °C 30 min | 0.58 | 14.6 |
| MW 4 min | 0.59 | 14.4 |
| MW 6 min | 0.59 | 14.4 |
| MW 8 min | 0.58 | 14.6 |

The close values suggest that microwave irradiation does not essentially change the crystal size of the nanocrystals.

Figure 2.17 shows the AFM surface morphology of mesoporous nc-$TiO_2$ films grown by conventional annealing and microwave irradiation. All the

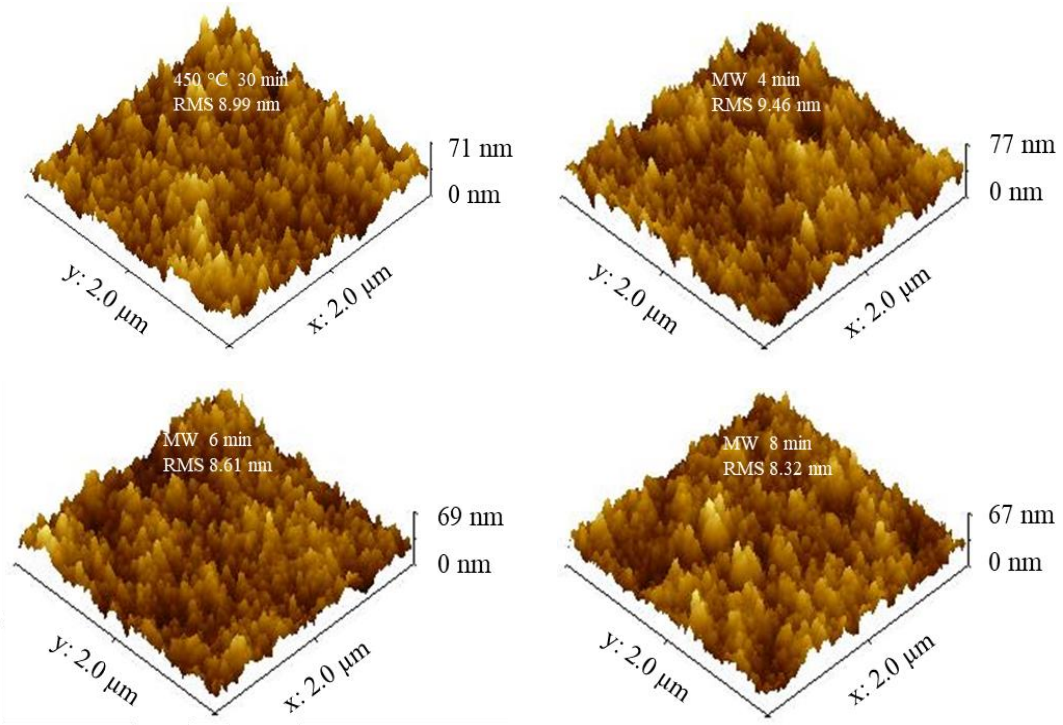


Figure 2.17. AFM surface morphologies of conventionally annealed and microwave irradiated mesoporous nc-$TiO_2$ films.

samples have essentially identical surface morphologies. To characterize surface roughness with AFM, the root mean square (RMS) is a widely used parameter [55, 56]. The measured RMS roughness was 8.99, 9.46, 8.61, and 8.32 nm for conventionally annealed (450 °C 30 min), and 4, 6, 8 min MW irradiated films respectively. There is somewhat small fraction of surface smoothness improvement with the increase of MW irradiation time which might be due to molecular vibration that helps to settle the molecules in a favorable position.

To observe the performance of films developed with MW irradiation compare to the conventionally annealed films, they were applied to fabricate DSSCs. The current density-voltage (J-V) characteristics of the fabricated cells are shown in Figure 2.18. Table 2.2 summarizes the photovoltaic performances of the cells. It is noticeable that there is a significant improvement in $J_{sc}$ and $V_{oc}$ from 4 min MW irradiation to 6 min MW irradiation, while there is little improvement in $J_{sc}$ and $V_{oc}$ from 6 to 8 min MW irradiation. The lower $J_{sc}$ at 4 min MW irradiation is likely due to trapped binder/organic molecules present in the film due to less calcination. The organic molecules hinder charge transport from dye to $TiO_2$ which affects the $J_{sc}$s.

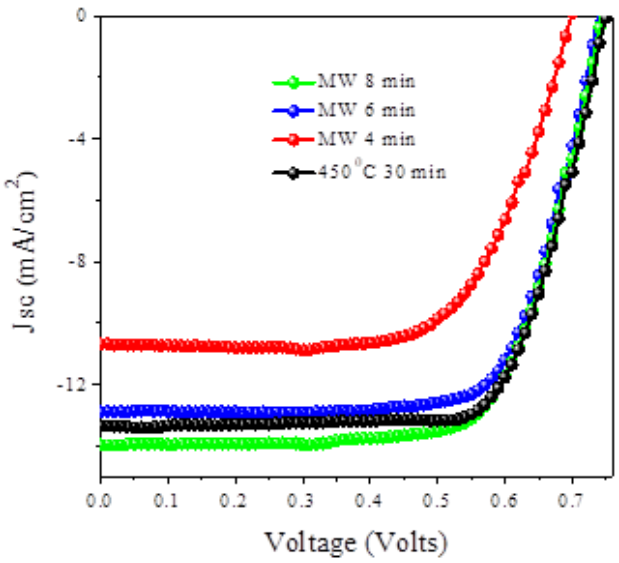


Figure 2.18. Cuttent density-voltage (J-V) characteristic curves of of DSSCs fabricated with mesoporous $TiO_2$ layer prepared at 30 min at 450 °C and 4, 6, 8 min MW

The lower $J_{sc}$ of the DSSC with 4 min MW film affects its overall performance. The maximum PCE of 4 min MW DSSC (~5%) was significantly low compared to the other cells whose maximum efficiency exceeds 7%.

Table 2.2. Current density-Voltage (J-V) characteristics of DSSCs fabricated with mesoporous $TiO_2$ prepared at 30 min 450 °C and 4, 6, 8 min MW irradiation.

| Photo anode heating time | $J_{sc}(mA/cm^2)$ | $V_{oc}$(Volt) | FF | η (%) | η (%) (max) |
|---|---|---|---|---|---|
| 450 °C 30 min | 13.51± 0.16 | 0.75±0.01 | 0.69±0.02 | 7.04±0.14 | 7.21 |
| MW 4 min | 10.73±0.18 | 0.69±0.02 | 0.61±0.03 | 4.57±0.35 | 4.95 |
| MW 6 min | 13.20±0.58 | 0.74±0.005 | 0.69±0.03 | 6.80±0.26 | 7.09 |
| MW 8 min | 14.09±0.21 | 0.75±0.01 | 0.68±0.01 | 7.16±0.09 | 7.25 |

To further ensure the charge transportation capability of the films, the $J_{sc}$s were calculated from the EQE. The EQE vs wavelength is shown in Figure 2.19.

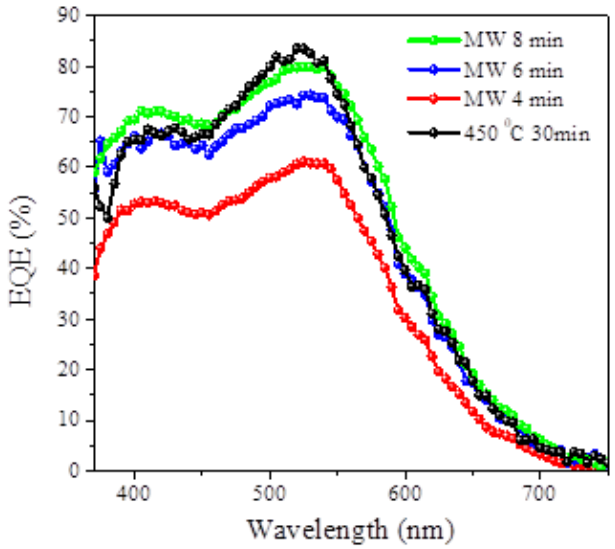


Figure 2.19. External quantum efficiency (EQE) response (a) J-V curves (b) EQE spectra.

The calculated $J_{sc}$ values are shown in Table 2.3. The $J_{sc}$s calculated from the IPCE curves are very close to the values obtained from the J-V curves as shown in Table 2.2. .

Table 2.3. $J_{sc}$ and IPCE of DSSCs fabricated with mesoporous $TiO_2$ prepared at 30 min 450 °C and 4, 6, 8 min MW irradiation.

| Photo-anode dye loading conditions | $J_{sc}(mA/cm^2)$ | Peak IPCE (%) |
|---|---|---|
| 450 °C 30 min | 13.34 | 83.52 |
| MW 4 min | 9.76 | 61.14 |
| MW 6 min | 12.41 | 74.36 |
| MW 8 min | 13.54 | 79.91 |

It is concluded that at 6-8 min MW irradiation nc-$TiO_2$ film property becomes similar to a 450 °C for 30 min sintered film.

**2.5 Conclusion**

This article demonstrates a novel technique of rapid (within 10 min) and low temperature ($\leq$ 260 °C) growth of nanocrystalline $TiO_2$ film using microwave irradiation on the FTO-coated glass substrate which would potentially replace conventional high temperature (450 °C) and long time (30-60 min) sintering. This achievement is attributed to vibration of molecules, close contact heat transfer to $TiO_2$ from the FTO which absorbs microwave irradiation excellently well, and solvent/ and organic binders' microwave absorption capability. This rapid and low temperature film growth technique can save significant amount of energy, and time and may pave the way for plastic based substrates. DSSCs fabricated with microwave developed films at an optimum deposition duration of just 8 minutes demonstrate an overall power conversion efficiency (PCE) of 7.16% as compared to 7.04% for conventionally fabricated DSSCs.

# Chapter 3. High-vacuum functionalized carboxylate deposition (FCD) of L1 and L2 dyes for efficient dye-sensitized solar cells

## 3.1 Introduction

### 3.1.1 Background

Dye sensitized solar cells (DSSCs) are considered as potential alternative to the silicon-based solar cells because of their low material cost, and ease of fabrication [8]. Moreover, they do not require glove-box conditions for their fabrication. Recently, ruthenium-based DSSCs have produced power conversion efficiencies (PCEs) more than 11% [57-59]. Although the advantages of DSSCs are promising, they still require some high-cost materials, including dyes which require complex synthetic and purification processes to produce highest efficiencies [8, 21]. Metal-free organic dyes have been extensively studied as alternative dyes for DSSCs. Metal-free organic dyes have advantages over the ruthenium-based sensitizers because of their tunable electrochemical and absorption properties, short synthesis routes, and relatively low cost [5, 60, 61]. Moreover, according to recent reports, several organic dyes have reached efficiencies more than 13% [62, 63]. However, the state-of-the-art dye loading technique, dip-coating constitutes a limiting step in fabrication of DSSCs, requiring the maximum portion of fabrication time (in average 16 h) [12]. The dip-coating method for dye loading has remained unchanged since the highly efficient (7.9%) DSSC was produced by O'regan and Gratzel in 1991 [19]. It is not only inefficient in terms of duration but also has other drawbacks, including requiring purified solvents, adjustment of solvents for specific sensitizers [64, 65]. Besides, a high concentration of dye is necessary and prolonged deposition time can easily lead to dye aggregation, degrading cell performance [4, 8].

Moreover, as the dye solution concentration changes after each dye bath of photoanodes, subsequent sensitization requires cautious duration of dipping. Functionalized Carboxylate Deposition (FCD), a vapor phase deposition technique was introduced as an alternative sensitization technique [12]. It significantly reduces dye loading time, allows more efficient use of dye material, and avoids the use of solvents.

### 3.1.2 Motivation

High-vacuum is expected to FCD high molecular weight dyes for quick sensitization of photoanodes leading to a fast and ultra-low cost DSSC fabrication without sacrificing the efficiency

### 3.1.3 Objectives

1. To improve the vacuum of the FCD system to achieve at least 0.1 mTorr within 10-15 minutes
2. Sensitize photo-anodes with organic dyes (Dye L1 and L2 as shown in Figure 3.1) of molecular weight more than 420 g/mole for DSSCs to achieve overall efficiency similar to or more than the dip-coated counterpart

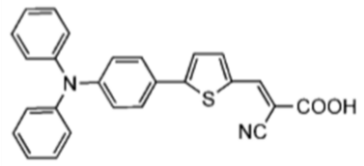


Dye L1

Molecular weight: 422.50 g/mol

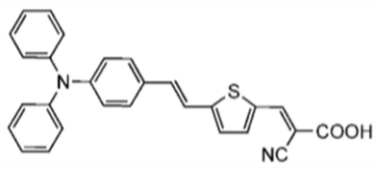


Dye L2

Molecular weight: 448.54 g/mol

Figure 3.1. Organic dyes L1: 5-[4-(diphenylamino)phenyl]thiophene-2-cyanoacrylic acid and L2: 3-(5-(4-(diphenylamino)styryl)thiophen-2-yl)-2-cyanoacrylic acid

## 3.2 Theory

### 3.2.1 Functionalized Carboxylate Deposition (FCD)

Functionalized Carboxylate Deposition (FCD) is a vapor phase deposition technique of organic dyes that was introduced as an alternative of the state-of-the-art dip-coating dye sensitization technique [12]. FCD significantly decreases the dye loading time by forming a self-assembled monolayer on the metal-oxide surface. A self-assembled monolayer (SAM) is a spontaneous adsorption of organic molecules on the surface.

Generally, hydroxyl groups prevail on a metal oxide surface for example Ti-OH on the outer surface of $TiO_2$ particles [66]. Usually, FCD molecules consist of three parts: an anchor group (R), a spacer/ pi-bridge, and an electron withdrawing functional group (for example -CN) in the α-position to a carboxyl group. When the dye molecules evaporated/sublimated they attach chemically with the surface sites through the carboxyl group as shown in Figure 3.2. In this way they form a covalent bond with the surface.

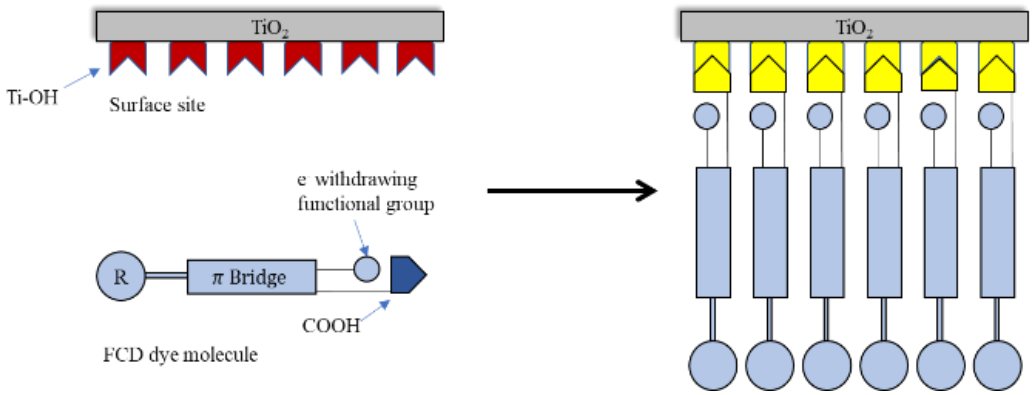


Figure 3.2. FCD dye molecules' attachment with the $TiO_2$ surface

When all of the surface sites attach with organic FCD dye molecules, the reaction stops which makes the process self-limiting [67]. The surface chemistry on the $TiO_2$ surface can be shown by the following reaction:

$$Ti\text{-}OH + R\text{-}COOH \longrightarrow Ti\text{-}COOR + H_2O$$

The major advantages of FCD over conventional dip-coating method are: 1) The process significantly decreases (more than 95%) dye loading time, 2) It avoids the use of solvent which is mandatory in dip-coating 3. It minimizes the use of dye to sensitize a photoanode.

### 3.2.2 DSSC construction and working principle

A typical DSSC consists of four main components (Figure 3.3): i) a photoanode, ii) a sensitizing dye, iii) an electrolyte or hole transporter, and iv) a counter-electrode [8]. Generally, the photoanode is prepared by sintering a mesoporous metal-oxide (e.g., $TiO_2$) layer on a transparent conducting oxide (TCO) coated glass substrate at 450-500 °C for 30-60 minutes. The counter-electrode is a thin platinum film on a TCO-coated substrate. The photoanode is sensitized with dye to chemisorb dye molecules onto $TiO_2$ nanoparticles. Tri-iodide/iodide electrolyte is injected between the dye-sensitized electrode and the counter-electrode.

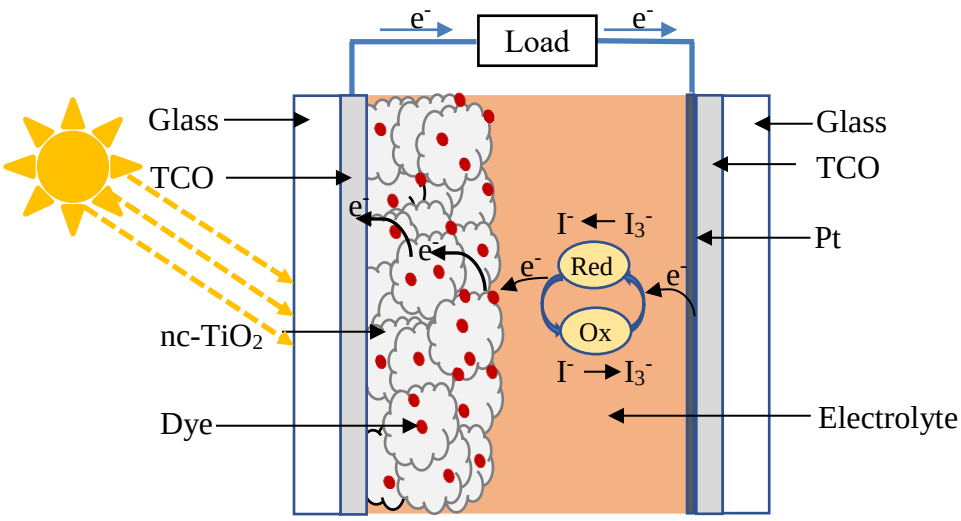


Figure 3.3. Construction and operation principle of a DSSC

The operation of a DSSC starts with the absorption of sunlight by dye sensitizers which are anchored to the surface of nc-$TiO_2$ particles. An absorbed photon excites electrons from the highest occupied molecular orbital (HOMO) to the lowest unoccupied molecular orbital (LUMO) of a dye molecule. The excited electrons transfers from the LUMO of dye to the conduction band of the $TiO_2$ which oxidizes the dye molecules. The injected electrons diffuse among the $TiO_2$ particles and are collected by the TCO. The electrons finally reach the counter electrode through the load in the outer circuit. The oxidized dye molecules ($D^+$) regain the lost electrons from $I^-$ of the electrolyte and $I^-$ becomes $I_3^-$.

$$2D^+ + 3I^- = 2D + I_3^- \quad (3.1)$$

The tri-iodide ions capture the electrons from the counter electrode and are reduced to $I^-$ ions.

$$I_3^- + 2e^- = 3I^- \quad (3.2)$$

The cycle is repeated with the electron injection from dye to $TiO_2$ and subsequent regeneration [68].

### 3.2.3 DSSC Characterization

#### 3.2.3.1 Current density, voltage, and power response of a solar cell

Figure 3.4 shows current-voltage response of a solar cell with and without illumination, and corresponding power-voltage relationship. The total power

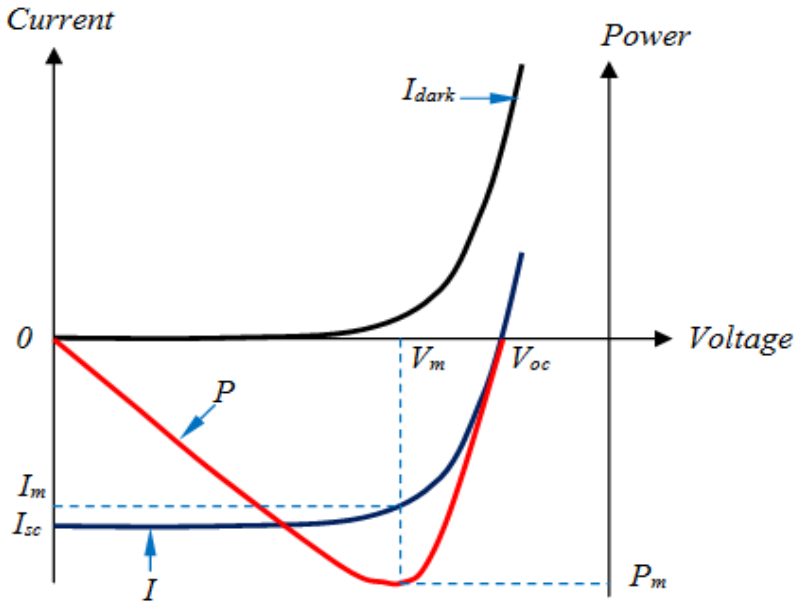


Figure 3.4. Current-voltage response of a solar cell with and without illumination and power-voltage relationship of a solar cell [24].

generated is the product of output current and voltage. The voltage $V_m$ and current $I_m$ corresponding to maximum power point gives maximum Power, $P_m = I_m V_m$.

The efficiency, $\eta$, of a solar cell is the ratio of maximum power delivered, $P_{m,}$ to the incident light power $P_s$,

$$\eta = \frac{I_m \ Vm}{Ps} \tag{3.3}$$

Fill factor, (FF) , gives the overall behavior of a solar cell and is the ratio of power available at maximum power point ($P_m$) to the product of open circuit voltage $V_{oc}$ and short circuit current ($I_{sc}$) [69] as,

$$FF = \frac{Pm}{Voc\ Isc} \tag{3.4}$$

3.2.3.2 External Quantum Efficiency (EQE)

External quantum efficiency (EQE) of a solar cell at a particular wavelength is the ratio of number of charge carriers (electrons) collected by the solar cell to the number of incident photons at that wavelength [70].

$$\text{EQE} = \frac{\text{number of electrons collected}}{\text{number of incident photons}}$$

Thus, both absorption of light and collection of charges affect the EQE. Recombination of charges results in drop of the EQE. Short circuit current of a solar cell can be calculated by integrating the EQE over the whole solar spectrum.

## 3.3 Experimental Procedures

The following tasks were performed to achieve the objectives of this chapter

1. Identify the major leakage area in the FCD system and seal the leaks to reach a pressure of 100 mTorr within 10 minutes with the new rotary vane pump.
2. Upgrade the FCD instrument with turbopump to ensure at least 0.1 mTorr pressure within 10-12 minutes.
3. Integrate a new digital mass flow controller (MFC) and a gate valve with the system to ensure fast response in pressure tuning and secure the turbopump respectively.
4. Sensitize photo-anodes with organic FCD dyes (dye L1, and L2) with upgraded FCD instrument in less than 30 minutes.
5. Optimize the FCD time for DSSCs' maximum power conversion efficiency (PCE) and compare it with the dip-coated counterpart.

### 3.3.1 Upgradation of FCD instrument

FCD is a vapor phase deposition technique where a high vacuum (upto 0.1 mTorr) is required to evaporate the FCD dye at a low sublimation/boiling temperature. The existed FCD system was able to provide around 500 mTorr. To reach the target vacuum within a short period of time the following steps were taken.

1. Identify the leaking area and seal it.
2. Install a turbo-pump (with gate valve) and integrate it with a new rotary vane pump.
3. Install a fast-responsive mass flow controller with integrated interface-able controller.

3.3.1.1 Identifying the leakage area

Different components (especially valves, baseplate, and clamps) of the system were tested with trial and error method to identify the major leakage areas. Major leak was found in the base-plate where the heater was screwed. With the base-plate connected with the vacuum chamber, the maximum vacuum reached in around 20 minutes was 480 mTorr as shown in Figure 3.5 (a). When the base-plate was replaced with the flat surface of the lab-jack (Figure 3.5 (b)), the maximum vacuum attained was 8.5 mTorr. This large pressure difference confirmed the leakage in the base-plate. Leak points were detected underneath the base plate (Figure 3.6 (a)) and then sealed with soldering lead (Figure 3.6 (b)). Figure 3.6 (c) shows the improved vacuum condition after leakage points were sealed. Later the baseplate was replaced with a hotplate.

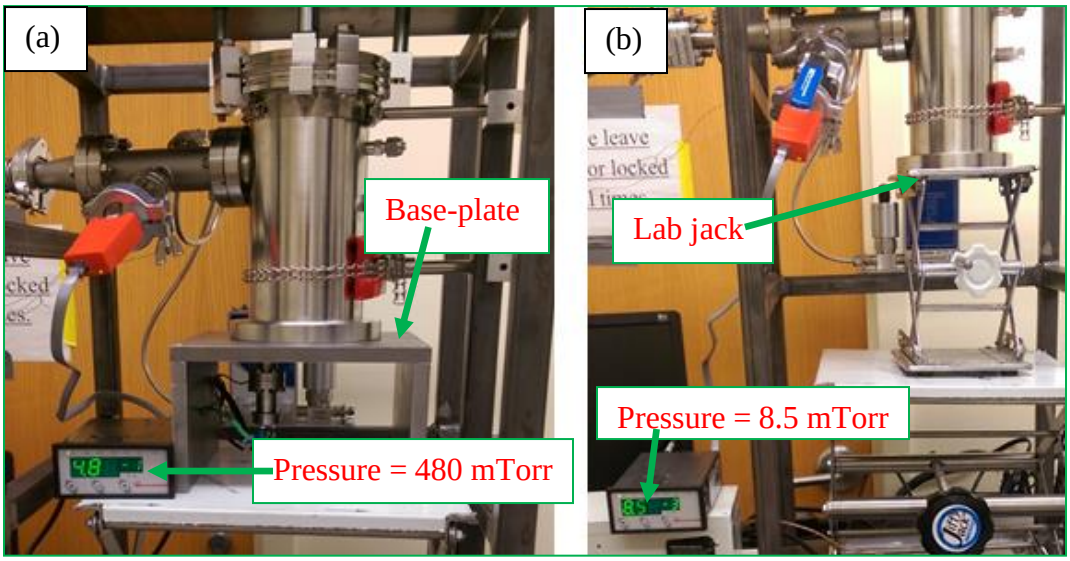


Figure 3.5. Identifying the major leakage area (testing of the base plate)

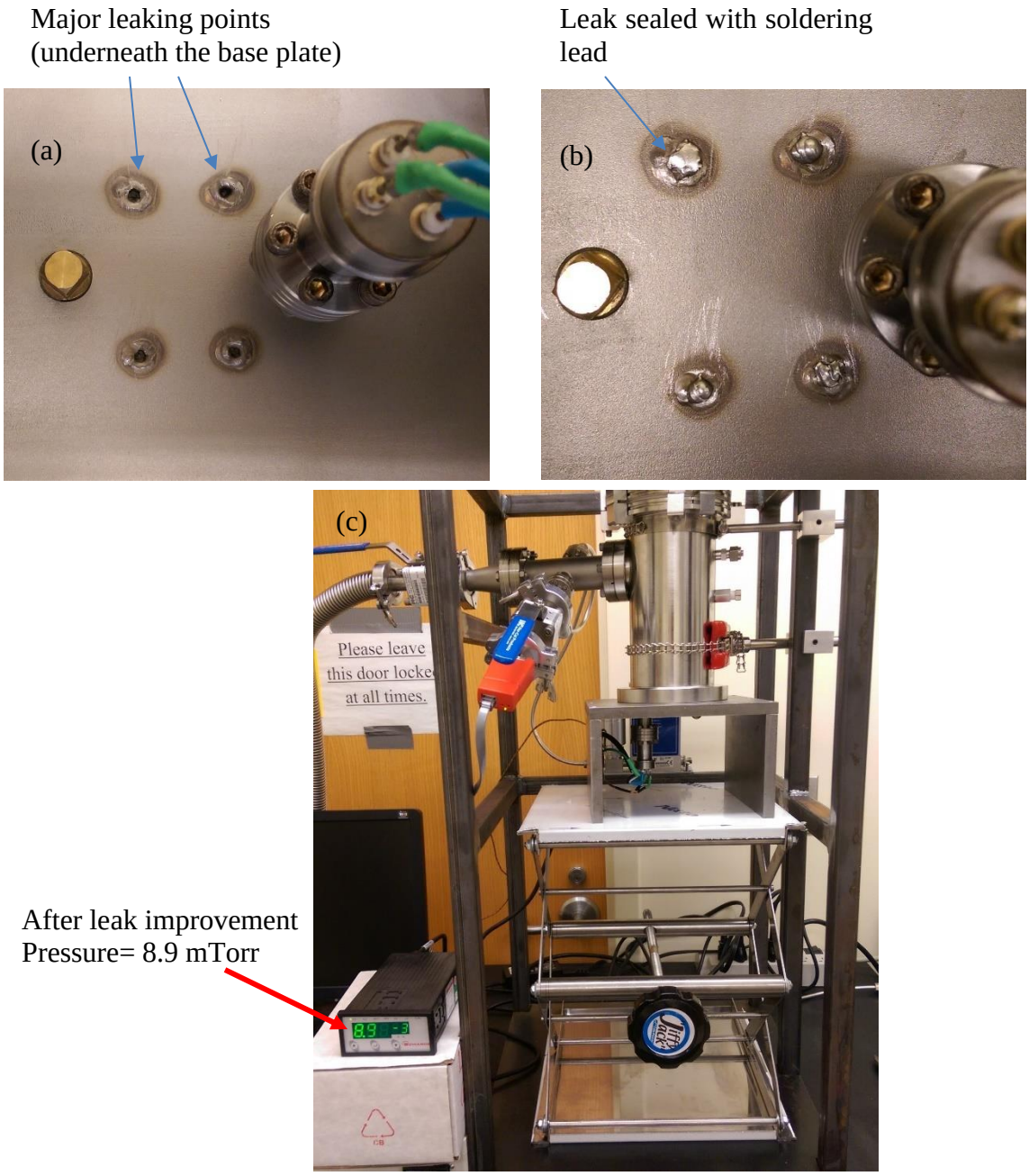


Figure 3.6. Identifying major leakage areas (a) Major leaking points (b) Leak points after soldering (c) Improved vacuum condition after sealing the major leaking points

3.3.1.2 Installing turbo pump

A ‘Pfeiffer HiPace 80 Compound Turbo Pump of KF-40 flange fitting’, a pump controller, and a ‘Pfeiffer PKR 251 Compact Full Range Pirani/Cold Cathode Gauge’ (Figure 3.7) were purchased from IdealVac.

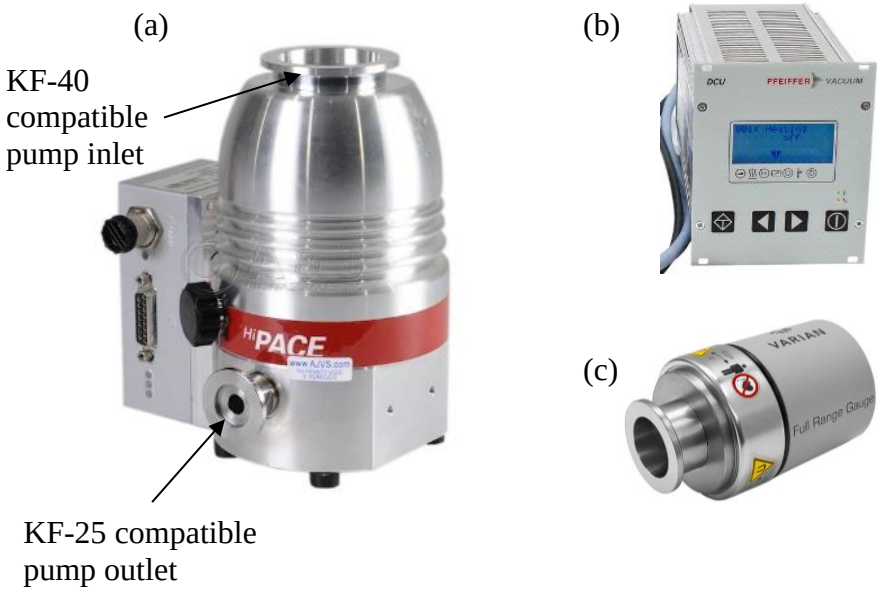


Figure 3.7. Turbopump and associated components (a) Peiffer HiPace 80 turbo pump (b) Pump controller (c) High vacuum pirani gauge

The outlet of the turbopump was connected with the inlet of a rotary vane pump (Maxima C Plus) (Figure 3.8) purchased from Fisher scientific. They were connected through Tee sections and valves.

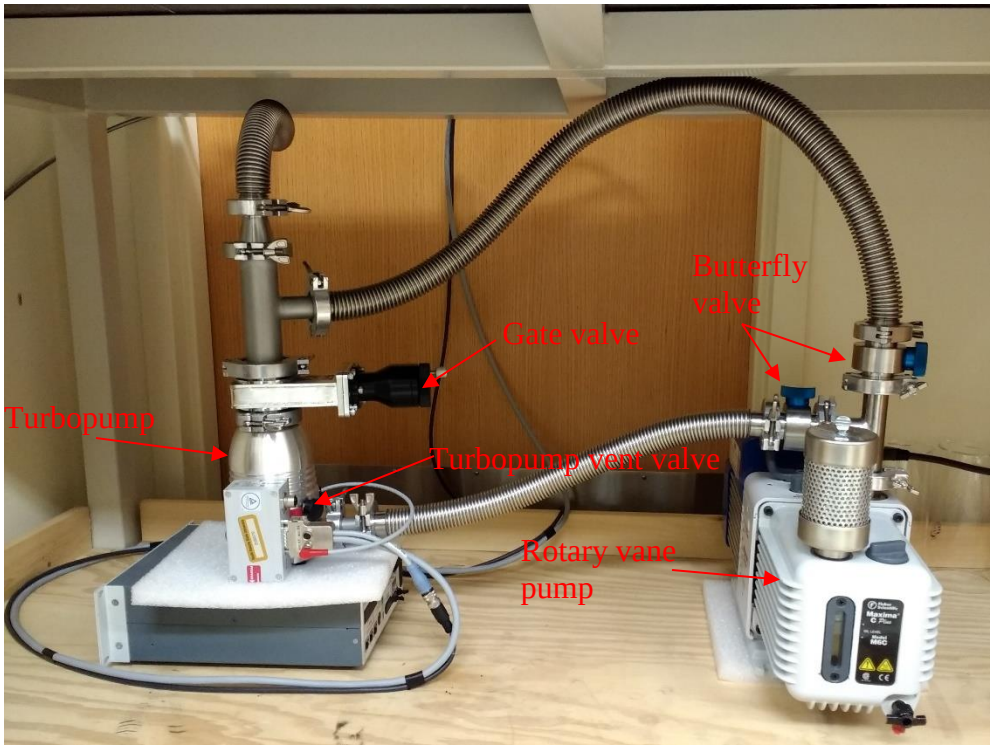


Figure 3.8. Connection of turbopump outlet with the rotary vane pump inlet

3.3.1.3 Installing new digital mass flow controller

A mass flow controller (Figure 3.9) was purchased from Alicat Scientific. This mass flow controller (MFC) has an integrated control panel and digital display unlike the previous unit. The integrated shut-off valve opens the outlet port when the pressure range is 80 to 150 psi. The principal purpose of the MFC is to precisely control Ar gas flow to the vacuum chamber before and after FCD.

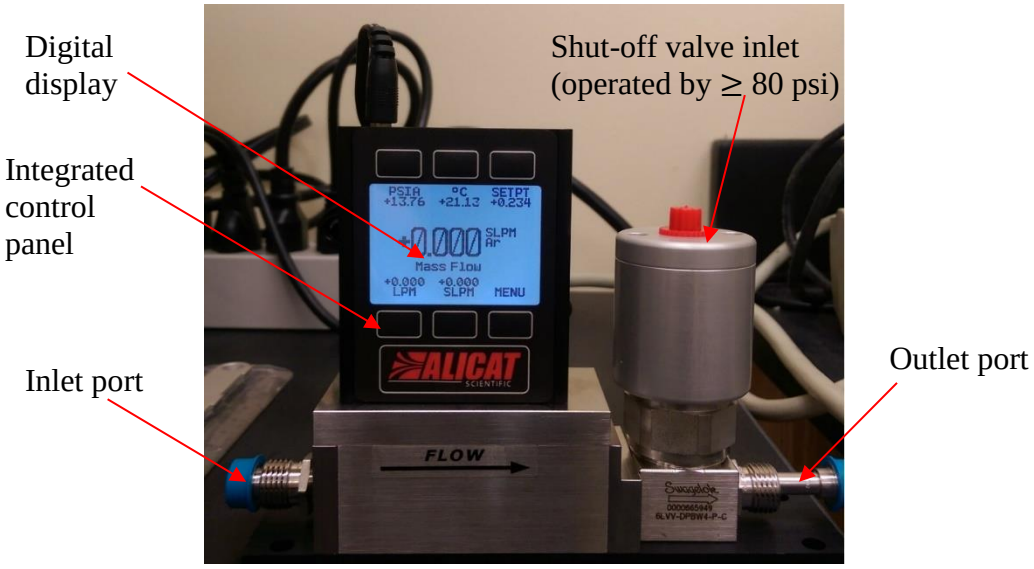


Figure 3.9. Alicat mass flow controller

3.3.4 Upgraded FCD system with components

Figure 3.10 shows the simplified schematic diagram of the upgraded FCD system and Figure 3.10 shows the photograph of the upgraded instrument with components.

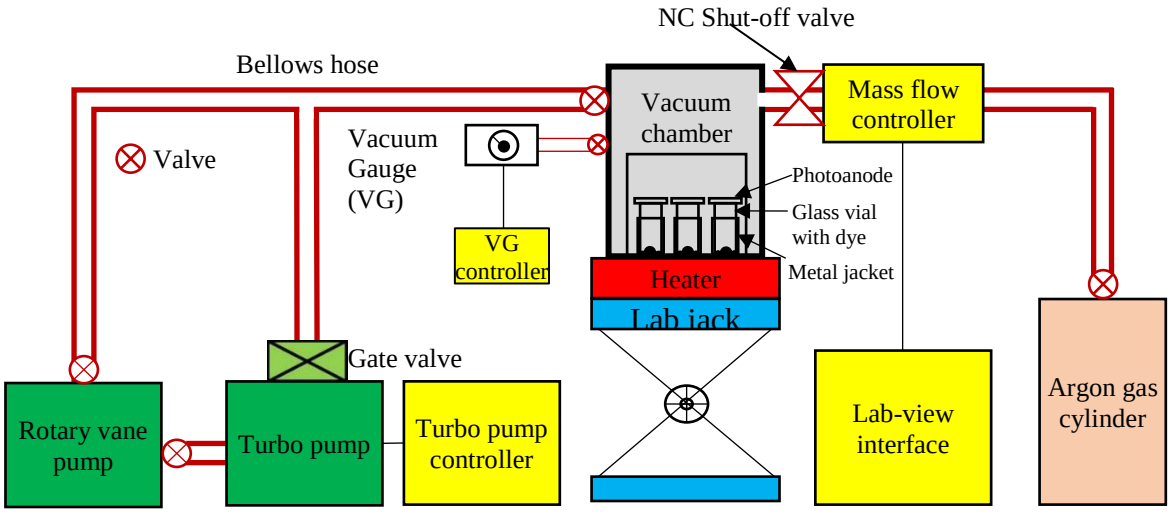


Figure 3.10. Schematic diagram of the upgraded FCD system

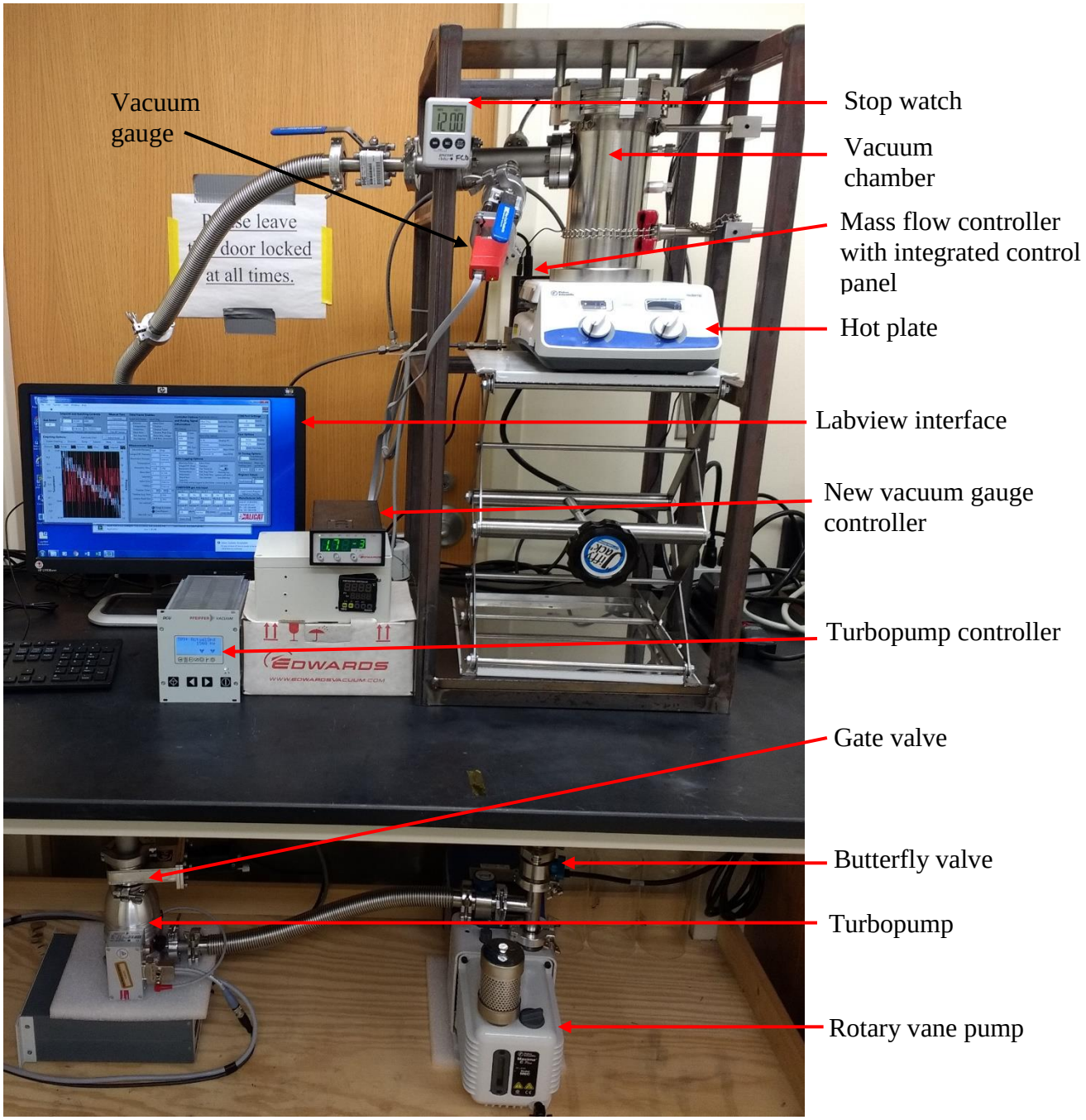


Figure 3.11. Upgraded FCD system

### 3.3.5 Fabrication and characterization of DSSCs using FCD and dip-coating

#### 3.3.5.1 Photoanode preparation

To prepare photoelectrodes, fluorine doped tin oxide (FTO) coated glass substrates (25 mm x 15 mm x 2.2 mm) were purchased from Hartford Glass Co., Indiana. Before any deposition, the substrates were cleaned by sonication with a soap water, deionized (DI) water, acetone, and iso-propanol (IPA) each for around 15 min. Then they were cleaned using UV exposure for 15 min. A layer of nanocrystalline $TiO_2$ of particle size 15-20 nm (Ti-Nanoxide T/SP), (purchased from Solaronix, Switzerland) was deposited with doctor blading and then sintered at 450 °C for around 30 minutes. The substrate was cooled down for 40 minutes followed by a second mesoporous layer deposited on the previous layer with same principle and then again sintered at 450 °C for ~30 minutes. A scattering layer of $TiO_2$ of particle size ~100 nm (Ti-Nanoxide R/SP-purchased from Solaronix, Switzerland), was deposited on the sintered mesoporous layer followed by a heating at 450 °C for ~30 minutes. After cooled, unassisted for around 40 minutes, the photoanodes were treated for 2 hours in a 0.1 M HCl solution. Then the photoanodes were dried using compressed nitrogen gas.

#### 3.3.5.2 Dye sensitization with dip-coat

For sensitization two organic FCD dyes L1 (5-[4-(diphenylamino)phenyl]thiophene-2-cyanoacrylic acid) and L2 (3-(5-(4-(diphenylamino)styryl)thiophen-2-yl)-2-cyanoacrylic acid) were purchased from Dyenamo, Sweden. To dip-coat, 0.3 mM dye solution (both for L1 and L2 dye) of anhydrous ethanol was prepared. The prepared photo-anodes were soaked in the dye

solution for 24 hours. After dye loading the photoanodes were rinsed with acetonitrile solution to remove any dye molecules weakly attached with the $TiO_2$ layer.

3.3.5.3 Dye sensitization with FCD

The prepared photoanodes was placed on top of a 9 mm x 30 mm shell vial after placing approximately 400 µg dye into the vial. Then the vial was placed into a metal jacket as shown in Figure 3.12. The whole assembly was

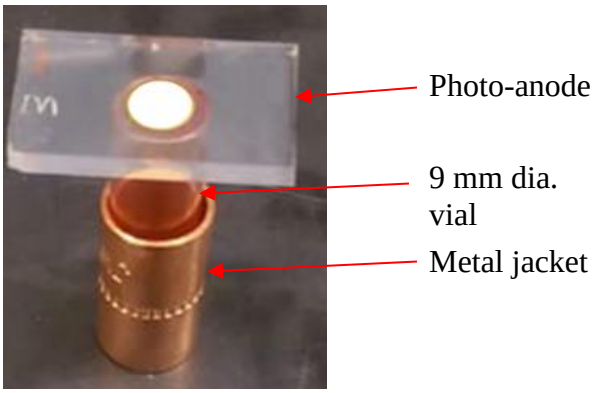


Figure 3.12. Placing the photo-anode for FCD sensitization

placed inside the vacuum chamber with the heater/hotplate underneath it. At first the chamber was evacuated with the rotary vane pump for 2 minutes, and then filled with Ar gas for approximately 1 minute. Then again, the chamber was evacuated with the rotary vane pump and turbo pump for approximately 10 minutes. When the pressure inside the chamber reached 3 mTorr, the heater was turned on to raise the temperature quickly to ~260 °C for L1 dye, and ~280 °C for L2 dye. The heater was turned off after a desired time duration and when the temperature dropped down to nearly 150 °C, the chamber was filled with Ar gas to reach the atmospheric pressure for the removal of the sensitized photo-anodes. After removal, the photo-electrodes were washed with ethanol and acetone

to wipe out any unanchored dye molecules. Then they were dried with compressed nitrogen gas.

3.3.5.4 DSSC fabrication

To prepare the counter electrode (CE) a platinum solution, Platisol T (from Solaronix, Switzerland) was spin-coated at 2000 rpm for ~10 s on top of the FTO substrates. Then the substrates were annealed at 450 °C for 15 min and then cooled down to room temperature. The CE was then sealed with the dye-sensitized photo-electrode with a thermal plastic with keeping a channel for the electrolyte. The $I_3^-/I^-$ electrolyte solution (Iodolyte HI-30 purchased from Solaronix, Switzerland) was injected through the channel. The channel openings were sealed using conventional hot glue gun.

3.3.6 Characterization and evaluation

3.3.6.1 Current density-voltage (J-V) characterization

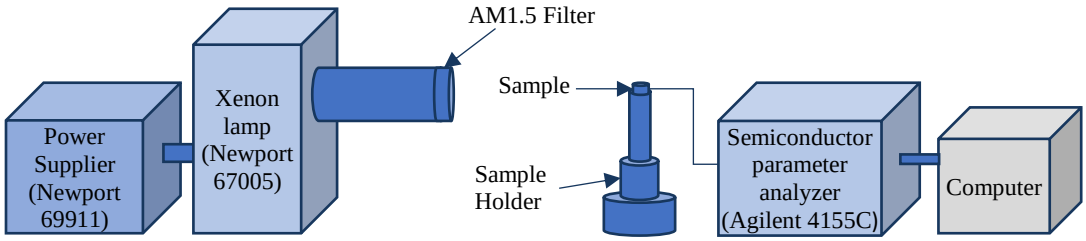


Figure 3.13. Schematic of current density-voltage measurement system

The schematic of the current density-voltage measurement system is shown in Figure 3.13. A Xenon arc lamp (Newport 67005) with an AM1.5 filter was used as a light source. To achieve a uniform illumination (without any fluctuation), first the lamp was turned on for ~15 minutes. A ‘Hamamatsu S1133’ photodetector was first placed in the sample holder to adjust the distance between solar simulator and photodetector to get a $J_{sc}$

that matches National Renewable Energy Laboratory data (NREL). All the measurements were performed at a light intensity of 1000 $W/m^2$. An Agilent 4155C was used as semiconductor parameter analyzer to apply bias voltage to the device and measure current from the device.

To test a DSSC, it was placed at same position in the sample holder by removing photodetector and bias voltage was swept from 0 V to 1 V at step of 10 mV to measure current at different voltage. Recorded J-V was plotted to obtain current density vs. voltage characteristics of the DSSC.

3.3.6.2 External Quantum Efficiency (EQE) measurement

The schematic of external quantum efficiency (EQE) measurement system is shown in Figure 3.14. Light from a Xenon lamp (Newport 67005) was focused to a Hamamatsu S1133 photodetector through an 'Oriel Monochromator 74001' and two focusing lenses. A PC connected with the monochromator controls the monochromator to pass the light from 350 nm to 800 nm at an interval of 5 nm. Trans-impedance amplifier amplified the current from S1133 detector to voltage ($V_{ref}$) which is recorded using semiconductor parameter analyzer (Agilent 4155C). To measure the EQE of a DSSC, the photodetector was replaced with the DSSC to the same place and procedure. Output voltage $V_{soalrcell}$ recorded at each wavelength. EQE of solar cell was calculated using NREL provided EQE data for S1133 photodetector, ($EQE_{ref}$) as $EQE_{solarcell} = (V_{solarcell} / V_{ref}) \times EQE_{ref.}$

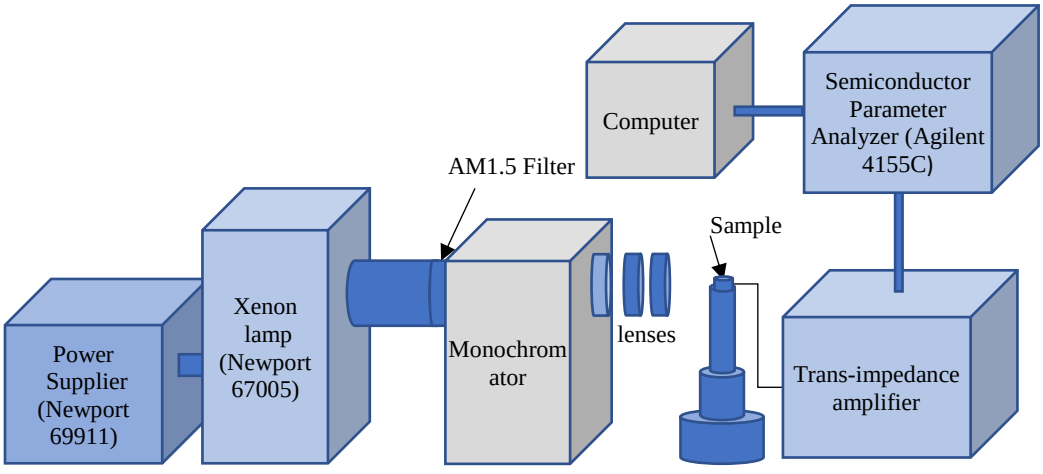


Figure 3.14. Schematic of external quantum efficiency measurement system.

## 3.4 Results and discussions

### 3.4.1 FCD of L1 dye

Figure 3.15 shows current density-voltage (J-V) characteristics curves of L1 dye based DSSCs fabricated with dip-coating and FCD at 260 °C for different durations. Table 3.1 summarizes the photovoltaic performance of DSSCs. Short circuit current density ($J_{sc}$) increased from 8.10 mA/cm$^2$ to 11.76 mA/cm$^2$ as FCD duration increased from 8 min to 16 min. Maximum $J_{sc}$ found at 16 min deposition may be due to optimum sensitization i.e. the monolayer formation of dye with $TiO_2$ particles. At 20 min deposition $J_{sc}$ decreases to 10.55 mA/cm$^2$ which might be due to the dye aggregation. While the open circuit voltage ($V_{oc}$) remained almost constant (~0.65 V) for the FCD cells, the fill-factor (FF) found at 16 min was 10% higher than that of the 8 min FCD cell. Due to the high $V_{oc}$ and FF the maximum efficiency was found in 16 min FCD cell which was even higher than the 24 h dip-coated cell. The dip-coated cell exhibited a PCE of 4.36% which was 15% less than the FCD optimized cell for which the PCE found 5.03%. However, with 0.68V the dip-coated cell shows a little higher $V_{oc}$ than any of the FCD cells (~0.65V). With L1 dye, the efficiency (5.03%) achieved with the FCD at the optimum deposition duration is very close to the current world record efficiency (5.20%) by dip-coating [8].

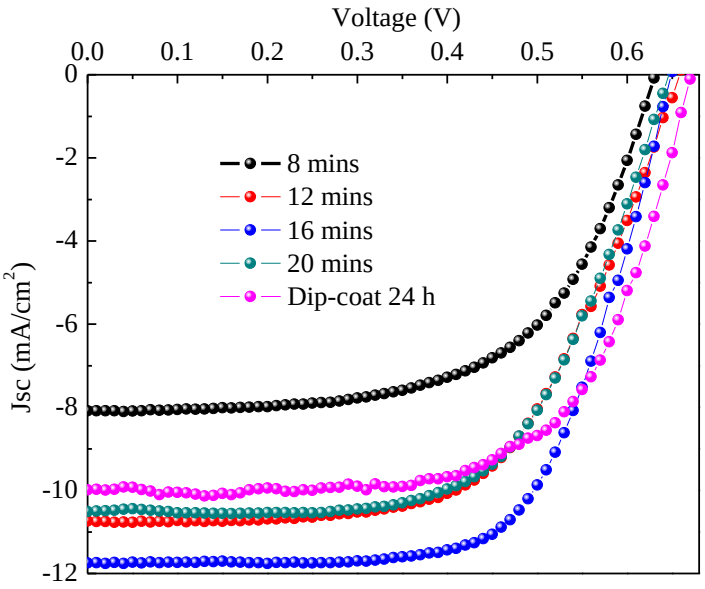


Figure 3.15. Current density-voltage (J-V) characteristics of L1 dye based DSSCs fabricated with FCD (at 260 °C) and dip-coating

Table 3.1. Current density-voltage (J-V) characteristics of L1 dye based DSSCs fabricated with FCD (at 260 °C) and dip-coating

| Photo anode sensitizing duration | $J_{sc}(mA/cm^2)$ | $V_{oc}(V)$ | FF | η (%) |
|---|---|---|---|---|
| FCD (8 min) | -8.10 | 0.64 | 0.60 | 3.08 |
| FCD (12 min) | -10.77 | 0.66 | 0.60 | 4.24 |
| FCD (16 min) | -11.76 | 0.65 | 0.66 | 5.03 |
| FCD (20 min) | -10.55 | 0.65 | 0.61 | 4.22 |
| Dip-coating 24 h | -10.13 | 0.68 | 0.63 | 4.36 |

The incident monochromatic photon-to-current conversion efficiency (IPCE) is shown in Figure 3.16 as a function of wavelength for the DSSCs fabricated with FCD at different deposition time and with dip-coating for 24 h. The maximum IPCEs for all the cells

found at around 420 nm of wavelength which is consistent with report of Hagberg et. al. [5]. IPCE increased from 69.15% at 8 min FCD to 85.51% at 16 min FCD and then again decreased to 81.45% at 20 min FCD. The $J_{sc}$ values calculated from IPCE spectra are shown in Table 3.2. These values are consistent with those measured from J−V curves.

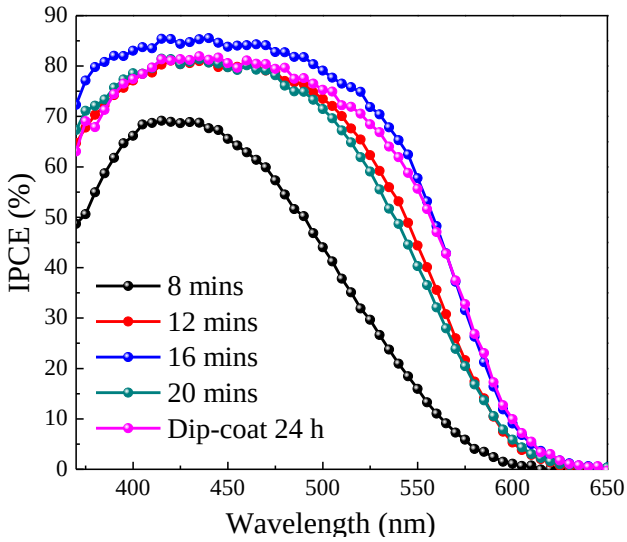


Figure 3.16. Incident photon-to-current efficiency (IPCE) spectra of L1 dye based DSSCs fabricated with FCD (at 260 °C) and dip-coating

Table 3.2. $J_{sc}$ and IPCE of L1 dye based DSSCs fabricated with FCD (at 260 °C) and dip-coating

| Photo-anode sensitizing duration | $J_{sc}(mA/cm^2)$ | Peak IPCE (%) |
|---|---|---|
| FCD (8 min) | -6.43 | 69.15 |
| FCD (12 min) | -9.82 | 81.06 |
| FCD (16 min) | -11.10 | 85.51 |
| FCD (20 min) | -9.65 | 81.45 |
| Dip-coating 24 h | -10.61 | 81.94 |

To study the amount of dye attachment at different time durations UV−Vis absorbance measurement was performed for dye solutions desorbed from photoanodes. After the efficiency was measured the DSSCs were deconstructed and the photoanodes were rinsed with acetonitrile to remove the residue of electrolyte attached with them and then dried with compressed $N_2$ gas.

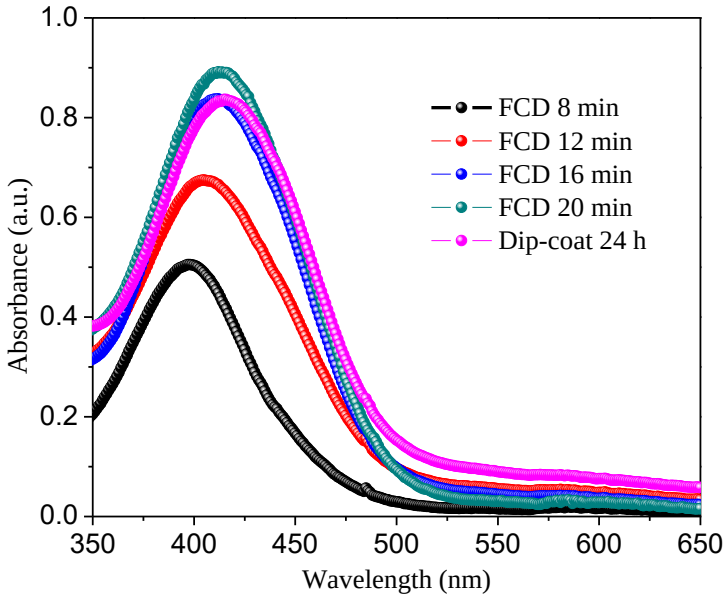


Figure 3.17. UV-Vis absorption spectra of L1 dye desorbed from the photoanodes

The dye attached with the photoanodes was extracted by dipping them in 3 mL 0.1M NaOH solution. The UV-Vis spectra of the extracted dye solution shown in Figure 3.17 ensures that the absorption peak intensity increased with the increment of FCD time. This implies the amount of dye loading increased with FCD duration. It is noticeable that similar amount of dye loaded for the dip-coated cell and 16 min FCD cell. At 20 min FCD slightly more amount of dye attached which might be the reason of slightly lower $J_{sc}$ at this duration than the optimum 16 min deposition.

3.4.2 FCD of L2 dye

Figure 3.18 shows current density-voltage (J-V) characteristics curves of L2 dye based DSSCs fabricated with dip-coating and FCD (at 280 °C) for different durations.

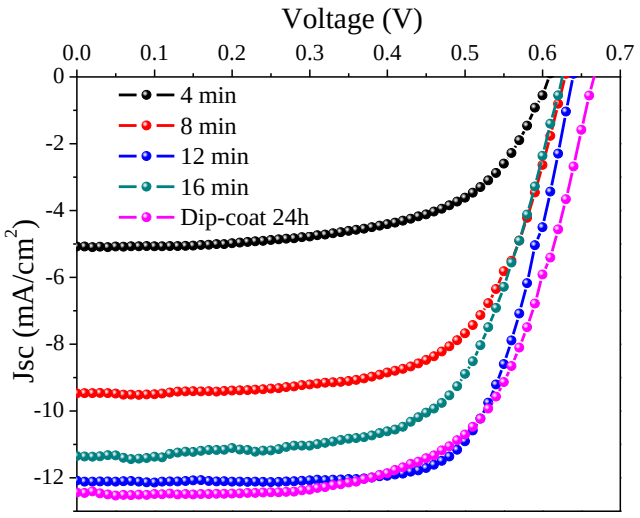


Figure 3.18. Current density-voltage (J-V) characteristics of L2 dye based DSSCs fabricated with FCD (at 280 °C) and dip-coating

Table 3.3 summarizes the photovoltaic performance of DSSCs. Short circuit current density ($J_{sc}$) increased from 5.10 mA/cm$^2$ at 4 min to 12.14 mA/cm$^2$ at 12 min through 9.52 mA/cm$^2$ at 8 min deposition. At 16 min deposition $J_{sc}$ decreases to 11.43 mA/cm$^2$ which might be due to the dye aggregation like in the case of L1 dye. While Open circuit voltage ($V_{oc}$) remains almost constant (~0.64 V) for the FCD cells the fill-factor (FF) found at 12 min was 70% which was even higher than dip-coated cell. The dip-coated cell exhibits a PCE of 5.35% which is slightly lower than the FCD optimized cell for which the PCE found 5.46% which very close to the current world record efficiency (5.94%) achieved by dip-coating [71].

Table 3.3. Current density-voltage (J-V) characteristics of L2 dye based DSSCs fabricated with FCD (at 280 °C) and dip-coating

| Photo-anode sensitizing duration | $J_{sc}(mA/cm^2)$ | $V_{oc}$(Volt) | FF | η (%) |
|---|---|---|---|---|
| FCD (4 min) | -5.10 | 0.61 | 0.60 | 1.86 |
| FCD (8 min) | -9.52 | 0.63 | 0.65 | 3.87 |
| FCD (12 min) | -12.14 | 0.64 | 0.70 | 5.46 |
| FCD (16 min) | -11.43 | 0.63 | 0.64 | 4.58 |
| Dip-coated 24 h | -12.53 | 0.67 | 0.64 | 5.35 |

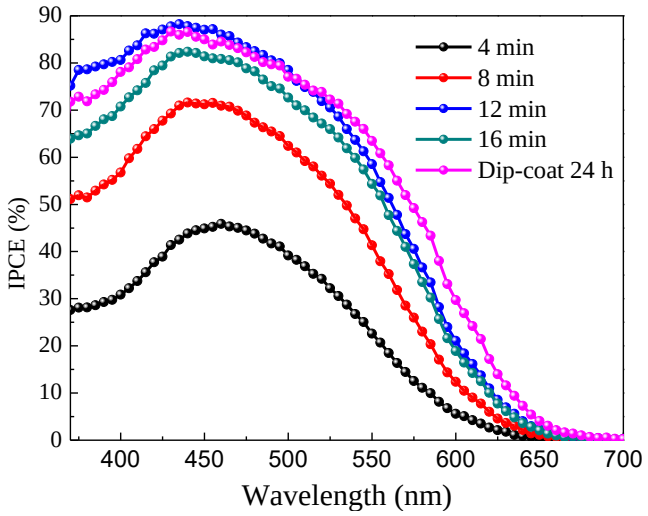


Figure 3.19. Incident photon-to-current efficiency (IPCE) spectra of L2 dye based DSSCs fabricated with FCD (at 280 °C) and dip-coating

The incident monochromatic photon-to-current conversion efficiency (IPCE) of the cells fabricated with L2 dye is shown in Figure 3.19.

The maximum IPCEs for all the cells found at around 440 nm of wavelength which is consistent with report of Hagberg et. al. [5]. IPCE increased from 45.87% at 4 min FCD

to 88.23% at 12 min FCD and then again decreased to 83.25% at 16 min FCD. The IPCE curve trends are with good agreement with the corresponding J-V curves.

Table 3.4. $J_{sc}$ and IPCE of L2 dye based DSSCs fabricated with FCD (at 260 °C) and dip-coating

| Photo-anode dye loading conditions | $J_{sc}(mA/cm^2)$ | Peak IPCE (%) |
|---|---|---|
| FCD (4 min) | -5.19 | 45.87 |
| FCD (8 min) | -8.84 | 71.60 |
| FCD (12 min) | -11.80 | 88.23 |
| FCD (16 min) | -10.92 | 83.25 |
| Dip-coated 24 h | -12.28 | 86.63 |

To study the amount of dye attachment at different time durations UV−vis absorbance measurement was performed for dye solutions desorbed from photoanodes. After the efficiency was measured the DSSCs were deconstructed and the photoanodes were rinsed with acetonitrile to remove the residue of electrolyte attached with them and then dried with compressed $N_2$ gas.

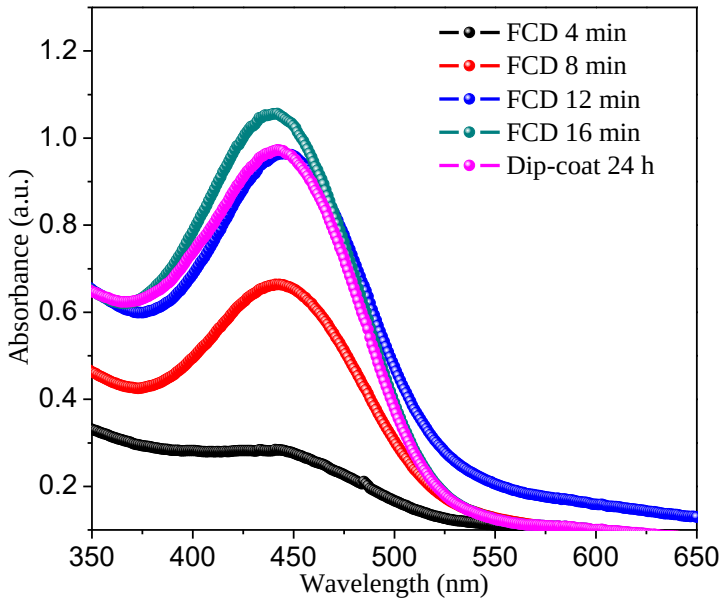


Figure 3.20. UV-Vis spectra of L2 dye desorbed from the photo-anodes

The dye attached with the photoanodes was extracted by dipping them in 3 mL 0.1 M NaOH solution. The UV-Vis spectra of the extracted dye solution shown in Figure 3.20 ensures that the absorption peak intensity increases with the increment of FCD time, which means the amount of dye loading increases with the deposition duration. It is noticeable that similar amount of dye loaded for the dip-coated cell and 12 min FCD cell. At 20 min FCD, slightly more amount of dye attached which might be reason of slightly lower $J_{sc}$ at this duration than the optimum 12 min deposition.

## 3.5 Conclusion

Using high vacuum (0.1 mTorr) FCD two organic dyes (dye L1 and L2) of molecular weights more than 420 g/mol were loaded on photoanodes within less than 30 minutes. The FCD DSSCs demonstrated higher power conversion efficiencies (5.03% and 5.46%, respectively) than their dip-coated counterparts (with PCEs 4.36% and 5.35%, respectively) while taking only ~3% sensitization time of dip-coating.

# Chapter 4. Summary and Conclusions

## 4.1 Summary

Current sources to meet the world energy demand are based on the fossil fuels. However, due to rapid depletion, fossil fuels will be unable to meet the ever-increasing energy demand in future. In addition, burning of fossil fuels impact negatively to the environment. So, renewable and clean energy sources need to be employed to encounter these challenges. Solar energy is a promising source of renewable energy which can be harnessed by using solar cells. Most of the commercially available solar cells are based on crystalline silicon which requires high cost for processing and production. Consequently, cost of electricity generated by silicon-based solar cells surpluses the price of grid electricity. As an alternative to the conventional silicon-based solar cells, dye-sensitized solar cells (DSSCs) have attracted copious attention due to their low production costs and good performance.

A typical DSSC consists of four basic parts: 1) a photoanode, 2) a sensitizing dye, 3) an electrolyte, and 4) a counter-electrode. The two major time-consuming steps DSSC fabrication are: 1) preparation of the photoanode and 2) sensitizing the photoelectrode with dye. The photoanode is prepared by depositing an nc-$TiO_2$ paste on a transparent conductive oxide (TCO) coated substrate followed by a high temperature sintering (450-500 °C) for 30-60 minutes. This high temperature and long-time sintering process limits the throughput and cost-effectiveness of this technology. Therefore, there is a need to develop technique to grow the films quickly.

As microwave irradiation can expedite reactions, it is widely used in synthesis of organic/inorganic materials. Researchers tried to grow $TiO_2$ film on TCO-coated substrates by direct microwave irradiation. However, direct exposure of the TCO-glasses in microwave results in immediate shattering of the substrates which was reported by Hart *et al.* and Uchida *et al.* As an alternative method, Elena Vigil *et al.* in 2000 and Reeja Jayan *et al.* in 2012 reported crystalline $TiO_2$ thin film growth on TCO-coated glass substrates in solution. However, the films were very nonuniform due to spontaneous growth in solution and it took similar time to conventional growth. In addition, sufficiently more material is required to grow films in solution than that is required in the film. Hence, a novel technique is necessary to grow films on TCO-coated glass substrates by direct microwave irradiation.

This thesis introduces a novel technique to rapidly form mesoporous $TiO_2$ films on FTO-coated glass substrates using microwave irradiation with essentially identical performance as conventional heating. In this technique the shattering problem of substrates was encountered. Microwave assisted films were prepared at low temperatures (< 260 °C) within less than 10 minutes and compared with the conventionally-developed films. DSSCs fabricated with 8 minutes of MW irradiated films show similar efficiencies with that of conventionally fabricated DSSCs. The method can save time, energy, and may pave the way for plastic-based electronics.

After the preparation of a photoanode it needs to be sensitized with dye. The state-of-the-art dye-sensitization method is dip-coating which consumes more than 80% of the fabrication time (16-24 h) of a DSSC. Thus, it remains as a limiting factor in DSSC fabrication since early 1990s when first modern DSSC was introduced. As an alternative

to the dip-coating, in 2015 Mallam and Baral *et al.* introduced functionalized carboxylate deposition (FCD), a vapor phase deposition technique. Successful FCD requires high vacuum to evaporate an organic dye at a lower temperature to form a monolayer with the nc-$TiO_2$ particles. With a custom built FCD instrument, Baral group reached around 500 mTorr and sensitized two organic dyes with it to fabricate DSSCs and got similar efficiencies to the dip-coating. However, those two dyes were of low molecular weight (< 341 g/mol) and were themselves inefficient. Generally, the efficient FCD dyes have higher molecular weight and they require high vacuum to sublimate at a lower temperature. Therefore, there was a need to upgrade the FCD instrument to achieve a higher vacuum at a shorter time to FCD efficient organic dyes.

To achieve the objectives, the FCD instrument was upgraded with turbopump, gate valve, and mass flow controller to acquire a vacuum of 0.1 mTorr within 12-15 minutes. With the upgraded FCD instrument two FCD compatible organic dyes (dye L1 and dye L2) were deposited to sensitize the photoanodes within less than 30 minutes. The efficiencies obtained for L1 and L2 dyes (5.03%, and 5.46% respectively) with FCD were higher than those of dip-coating (4.36%, and 5.35% respectively) while FCD takes less than 3% sensitization time of the conventional dip-coating method.

## 4.2 Conclusions

This thesis introduces a novel technique to rapidly grow nc-$TiO_2$ films on FTO-coated glass substrates using microwave irradiation. Microwave-assisted films were prepared at low temperatures (< 260 °C) within less than 10 minutes. DSSCs fabricated with 8 minutes microwave-irradiated films show similar efficiencies (7.16%) with that of conventionally-fabricated DSSCs (with an efficiency of 7.04%). Besides saving time, and

energy compared to its counterpart, this approach may pave the way of plastic-based electronics. This thesis also demonstrates the rapid (< 30 minutes) loading of two functionalized carboxylate deposition (FCD) dyes through high vacuum (< 0.1 mTorr) FCD. The efficiency achieved with the FCD DSSCs were higher than dip-coated DSSCs. If combined, these two techniques can save more than 90% fabrication time for future ultra-low cost DSSCs.

## 4.3 Future works

1) Sensitize the microwave-developed photoanodes using functionalized carboxylate deposition (FCD) and evaluate their performances.

2) Fabricate perovskite solar cells using microwave-developed thin mesoporous layer and compare their performances with conventionally fabricated perovskite cells.

3) Deposit higher-efficient FCD dyes using FCD method to fabricate DSSCs and compare their performances with dip-coated DSSCs.

## REFERENCES


[1] R. A. Kerr, "Global warming is changing the world," Science, vol. 316, no. 5822, pp. 188-190, 2007.

[2] N. S. Lewis and G. Crabtree, "Basic research needs for solar energy utilization: report of the basic energy sciences workshop on solar energy utilization, April 18-21, 2005," ed: US Department of Energy, Office of Basic Energy Science, 2005.

[3] M. Grätzel, "Photoelectrochemical cells," nature, vol. 414, no. 6861, p. 338, 2001.

[4] Z. Ning, Y. Fu, and H. Tian, "Improvement of dye-sensitized solar cells: what we know and what we need to know," Energy & Environmental Science, vol. 3, no. 9, pp. 1170-1181, 2010.

[5] D. P. Hagberg et al., "Tuning the HOMO and LUMO energy levels of organic chromophores for dye sensitized solar cells," The Journal of organic chemistry, vol. 72, no. 25, pp. 9550-9556, 2007.

[6] Y. Xie et al., "Electrolyte Effects on Electron Transport and Recombination at ZnO Nanorods for Dye-Sensitized Solar Cells," The Journal of Physical Chemistry C, vol. 114, no. 41, pp. 17880-17888, 2010/10/21 2010.

[7] Y. Xue et al., "Nitrogen-doped graphene foams as metal-free counter electrodes in high-performance dye-sensitized solar cells," Angewandte Chemie International Edition, vol. 51, no. 48, pp. 12124-12127, 2012.

[8] A. Mishra, M. K. Fischer, and P. Bäuerle, "Metal-free organic dyes for dye-sensitized solar cells: From structure: Property relationships to design rules," Angewandte Chemie International Edition, vol. 48, no. 14, pp. 2474-2499, 2009.

[9] J. N. Hart, D. Menzies, Y.-B. Cheng, G. P. Simon, and L. Spiccia, "Microwave processing of TiO2 blocking layers for dye-sensitized solar cells," Journal of sol-gel science and technology, vol. 40, no. 1, pp. 45-54, 2006.

[10] A. Gurung, H. Elbohy, D. Khatiwada, A. F. Mitul, and Q. Qiao, "A Simple Cost-Effective Approach to Enhance Performance of Bifacial Dye-Sensitized Solar Cells," IEEE Journal of Photovoltaics, vol. 6, no. 4, pp. 912-917, 2016.

[11] C. J. Barbe et al., "Nanocrystalline titanium oxide electrodes for photovoltaic applications," Journal of the American Ceramic Society, vol. 80, no. 12, pp. 3157-3171, 1997.

[12] V. Mallam et al., "Functionalized Carboxylate Deposition for rapid sensitization of dye-sensitized solar cells," Solar Energy, vol. 126, pp. 128-136, 2016.

[13] B. O'regan and M. Grfitzeli, "A low-cost, high-efficiency solar cell based on dye-sensitized," nature, vol. 353, p. 24, 1991.

[14] D. H. Kim, M. D. Losego, Q. Peng, and G. N. Parsons, "Atomic Layer Deposition for Sensitized Solar Cells: Recent Progress and Prospects," Advanced Materials Interfaces, vol. 3, no. 21, 2016.

[15] L. Bedikyan, S. Zakhariev, and M. Zakharieva, "Titanium dioxide thin films: preparation and optical properties," Journal of Chemical Technology and Metallurgy, vol. 48, no. 6, pp. 555-558, 2013.

[16] E. Vigil, L. Saadoun, J. A. Ayllón, X. Domènech, I. Zumeta, and R. Rodríguez-Clemente, "TiO 2 thin film deposition from solution using microwave heating," Thin Solid Films, vol. 365, no. 1, pp. 12-18, 2000.

[17] J. Hart, Y.-B. Cheng, G. Simon, and L. Spiccia, "Challenges of producing TiO2 films by microwave heating," Surface and Coatings Technology, vol. 198, no. 1-3, pp. 20-23, 2005.
[18] B. Reeja-Jayan, K. L. Harrison, K. Yang, C.-L. Wang, A. Yilmaz, and A. Manthiram, "Microwave-assisted low-temperature growth of thin films in solution," Scientific reports, vol. 2, p. 1003, 2012.
[19] B. O'regan and M. Grätzel, "A low-cost, high-efficiency solar cell based on dye-sensitized colloidal TiO2 films," nature, vol. 353, no. 6346, p. 737, 1991.
[20] T. W. Hamann, R. A. Jensen, A. B. Martinson, H. Van Ryswyk, and J. T. Hupp, "Advancing beyond current generation dye-sensitized solar cells," Energy & Environmental Science, vol. 1, no. 1, pp. 66-78, 2008.
[21] S. Ahmad, E. Guillén, L. Kavan, M. Grätzel, and M. K. Nazeeruddin, "Metal free sensitizer and catalyst for dye sensitized solar cells," Energy & Environmental Science, vol. 6, no. 12, pp. 3439-3466, 2013.
[22] S. Mathew et al., "Dye-sensitized solar cells with 13% efficiency achieved through the molecular engineering of porphyrin sensitizers," Nat Chem, Article vol. 6, no. 3, pp. 242-247, 03//print 2014.
[23] S. Baral, "Study of TiO2 Films Sensitized with Dye by Functionalized Carboxylate Deposition for Dye Sensitized Solar Cells," 2014.
[24] S. Gyawali, "Functionalized Carboxylate Deposition (FCD) of Organic Molecules for Highly Efficient DSSC'S," 2015.
[25] A. L. Linsebigler, G. Lu, and J. T. Yates Jr, "Photocatalysis on TiO2 surfaces: principles, mechanisms, and selected results," Chemical reviews, vol. 95, no. 3, pp. 735-758, 1995.
[26] B. O'regan and M. Grätzel, "A low-cost, high-efficiency solar cell based on dye-sensitized colloidal TiO 2 films," nature, vol. 353, no. 6346, pp. 737-740, 1991.
[27] I. P. Parkin and R. G. Palgrave, "Self-cleaning coatings," Journal of Materials Chemistry, vol. 15, no. 17, pp. 1689-1695, 2005.
[28] H. Tang, K. Prasad, R. Sanjines, and F. Levy, "TiO2 anatase thin films as gas sensors," Sensors and Actuators B: Chemical, vol. 26, no. 1-3, pp. 71-75, 1995.
[29] C. Natarajan, N. Fukunaga, and G. Nogami, "Titanium dioxide thin film deposited by spray pyrolysis of aqueous solution," Thin Solid Films, vol. 322, no. 1, pp. 6-8, 1998.
[30] H. Y. Liu, S. H. Hong, W. C. Sun, S. Y. Wei, and S. M. Yu, "TiO<sub>2</sub>-Based Metal–Semiconductor–Metal Ultraviolet Photodetectors Deposited by Ultrasonic Spray Pyrolysis Technique," IEEE Transactions on Electron Devices, vol. 63, no. 1, pp. 79-85, 2016.
[31] P. Lidström, J. Tierney, B. Wathey, and J. Westman, "Microwave assisted organic synthesis—a review," Tetrahedron, vol. 57, no. 45, pp. 9225-9283, 2001.
[32] E. M. M. Flores, Microwave-assisted sample preparation for trace element determination. Newnes, 2014.
[33] S. Uchida, M. Tomiha, N. Masaki, A. Miyazawa, and H. Takizawa, "Preparation of TiO2 nanocrystalline electrode for dye-sensitized solar cells by 28 GHz microwave irradiation," Solar Energy Materials and Solar Cells, vol. 81, no. 1, pp. 135-139, 2004.

[34] T. Kim, J. Lee, and K.-H. Lee, "Microwave heating of carbon-based solid materials," Carbon letters, vol. 15, no. 1, pp. 15-24, 2014.
[35] S. Bagheri, Z. A. M. Hir, A. T. Yousefi, and S. B. A. Hamid, "Progress on mesoporous titanium dioxide: synthesis, modification and applications," Microporous and Mesoporous Materials, vol. 218, pp. 206-222, 2015.
[36] H. S. University, "Microwave Remote Sensing Overview," May 11, 2018.
[37] M. Baghbanzadeh, L. Carbone, P. D. Cozzoli, and C. O. Kappe, "Microwave-assisted synthesis of colloidal inorganic nanocrystals," Angewandte Chemie International Edition, vol. 50, no. 48, pp. 11312-11359, 2011.
[38] J. M. Hill and M. J. Jennings, "Formulation of model equations for heating by microwave radiation," Applied mathematical modelling, vol. 17, no. 7, pp. 369-379, 1993.
[39] MKS, "Microwave Heating Applications  Part 1: Fundamentals," May 12, 2018.
[40] D. A. Skoog, F. J. Holler, and S. R. Crouch, Principles of instrumental analysis. Cengage learning, 2017.
[41] J. A. Soares, "Introduction to Optical Characterization of Materials," in Practical Materials Characterization: Springer, 2014, pp. 43-92.
[42] P. Graves and D. Gardiner, "Practical Raman Spectroscopy," ed: Springer, 1989.
[43] HAMAMATSU. (May 10, 2018). Surface-enhanced Raman spectroscopy, . Available: https://www.hamamatsu.com/eu/en/technology/lifephotonics/environment/SuperiorDetectionOfDiverseChemicals/index.html
[44] Wikipedia. (May 10, 2018). X-ray crystallography. Available: https://en.wikipedia.org/wiki/X-ray_crystallography
[45] (May 10, 2018). X-ray diffraction. Available: http://www.veqter.co.uk/residual-stress-measurement/x-ray-diffraction
[46] P. Eaton and P. West, Atomic force microscopy. Oxford University Press, 2010.
[47] G. Haugstad, Atomic force microscopy: understanding basic modes and advanced applications. John Wiley & Sons, 2012.
[48] S. Uchida, M. Tomiha, H. Takizawa, and M. Kawaraya, "Flexible dye-sensitized solar cells by 28 GHz microwave irradiation," Journal of Photochemistry and Photobiology A: Chemistry, vol. 164, no. 1-3, pp. 93-96, 2004.
[49] M. Vollmer, "Physics of the microwave oven," Physics Education, vol. 39, no. 1, p. 74, 2004.
[50] R. Valaski, C. Canestraro, L. Micaroni, R. Mello, and L. Roman, "Organic photovoltaic devices based on polythiophene films electrodeposited on FTO substrates," Solar energy materials and solar cells, vol. 91, no. 8, pp. 684-688, 2007.
[51] P. Joshi, Y. Xie, M. Ropp, D. Galipeau, S. Bailey, and Q. Qiao, "Dye-sensitized solar cells based on low cost nanoscale carbon/TiO 2 composite counter electrode," Energy & Environmental Science, vol. 2, no. 4, pp. 426-429, 2009.
[52] E. Grant and B. J. Halstead, "Dielectric parameters relevant to microwave dielectric heating," Chemical society reviews, vol. 27, no. 3, pp. 213-224, 1998.
[53] D. Michael P áMingos, "Tilden Lecture. Applications of microwave dielectric heating effects to synthetic problems in chemistry," Chemical Society Reviews, vol. 20, no. 1, pp. 1-47, 1991.

[54] N. Wetchakun, B. Incessungvorn, K. Wetchakun, and S. Phanichphant, "Influence of calcination temperature on anatase to rutile phase transformation in TiO2 nanoparticles synthesized by the modified sol–gel method," Materials Letters, vol. 82, pp. 195-198, 2012/09/01/ 2012.
[55] R. Mechiakh, N. B. Sedrine, J. B. Naceur, and R. Chtourou, "Elaboration and characterization of nanocrystalline TiO2 thin films prepared by sol–gel dip-coating," Surface and Coatings Technology, vol. 206, no. 2-3, pp. 243-249, 2011.
[56] M. Zhang, G. Lin, C. Dong, and L. Wen, "Amorphous TiO2 films with high refractive index deposited by pulsed bias arc ion plating," Surface and Coatings Technology, vol. 201, no. 16-17, pp. 7252-7258, 2007.
[57] S. Mathew et al., "Dye-sensitized solar cells with 13% efficiency achieved through the molecular engineering of porphyrin sensitizers," Nature Chemistry, Article vol. 6, p. 242, 02/02/online 2014.
[58] M. K. Nazeeruddin et al., "Combined experimental and DFT-TDDFT computational study of photoelectrochemical cell ruthenium sensitizers," Journal of the American Chemical Society, vol. 127, no. 48, pp. 16835-16847, 2005.
[59] C.-Y. Chen et al., "Highly efficient light-harvesting ruthenium sensitizer for thin-film dye-sensitized solar cells," ACS nano, vol. 3, no. 10, pp. 3103-3109, 2009.
[60] H. Tian and F. Meng, "Organic Photovoltaics: Mechanisms," Materials, and Devices, CRC, London, p. 313, 2005.
[61] C. J. Liang, Y. J. Lin, Y. S. Yen, J. T. Lin, and M. C. P. Yeh, "Metal-Free Indeno [2, 1-b] thiophene-Based Sensitizers for Dye-Sensitized Solar Cells," Asian Journal of Organic Chemistry, vol. 5, no. 6, pp. 801-811, 2016.
[62] Z. Yao et al., "Dithienopicenocarbazole as the kernel module of low-energy-gap organic dyes for efficient conversion of sunlight to electricity," Energy & Environmental Science, vol. 8, no. 11, pp. 3192-3197, 2015.
[63] K. Kakiage, Y. Aoyama, T. Yano, K. Oya, J.-i. Fujisawa, and M. Hanaya, "Highly-efficient dye-sensitized solar cells with collaborative sensitization by silyl-anchor and carboxy-anchor dyes," Chemical Communications, vol. 51, no. 88, pp. 15894-15897, 2015.
[64] H. Tian, X. Yang, R. Chen, R. Zhang, A. Hagfeldt, and L. Sun, "Effect of different dye baths and dye-structures on the performance of dye-sensitized solar cells based on triphenylamine dyes," The Journal of Physical Chemistry C, vol. 112, no. 29, pp. 11023-11033, 2008.
[65] P. Shen et al., "Efficient triphenylamine dyes for solar cells: effects of alkyl-substituents and π-conjugated thiophene unit," Dyes and Pigments, vol. 83, no. 2, pp. 187-197, 2009.
[66] S. M. George, B. Yoon, and A. A. Dameron, "Surface Chemistry for Molecular Layer Deposition of Organic and Hybrid Organic−Inorganic Polymers," Accounts of Chemical Research, vol. 42, no. 4, pp. 498-508, 2009/04/21 2009.
[67] B. Yoon, J. L. O'Patchen, D. Seghete, A. S. Cavanagh, and S. M. George, "Molecular Layer Deposition of Hybrid Organic-Inorganic Polymer Films using Diethylzinc and Ethylene Glycol," Chemical Vapor Deposition, vol. 15, no. 4-6, pp. 112-121, 2009.
[68] A. Jena et al., "Dye sensitized solar cells: a review," Transactions of the Indian Ceramic Society, vol. 71, no. 1, pp. 1-16, 2012.

[69] wikipedia. (4/9/2015). solar cell efficiency. Available: http://en.wikipedia.org/wiki/Solar_cell_efficiency
[70] wikipedia. (4/9/2015). Quantam Efficiency. Available: http://en.wikipedia.org/wiki/Quantum_efficiency
[71] D. P. Hagberg et al., "Molecular engineering of organic sensitizers for dye-sensitized solar cell applications," Journal of the American Chemical Society, vol. 130, no. 19, pp. 6259-6266, 2008.